



1 **Title: Acidification in coastal waters of Adélie Land, Antarctica (1985-2025)**

2

3 Nicolas Metzl¹, Bronte Tilbrook^{2,3}, John Akl², Craig Neill², Alexandra Aymard¹, Claire Lo Monaco¹,
4 Gilles Reverdin¹, Jean-Baptiste Sallée¹, Aude Barton⁴, Frédéric Chevallier⁴, Marion Gehlen⁴

5

6 1 Laboratoire LOCEAN/IPSL, Sorbonne Université-CNRS-IRD-MNHN, Paris, 75005, France

7 2 CSIRO Environment, Castray Esplanade, Hobart, TAS 7004, Australia

8 3 Australian Antarctic Partnership Program, University of Tasmania, Hobart, TAS, Australia

9 4 Laboratoire LSCE/IPSL, CEA-CNRS-UVSQ, Université Paris-Saclay Gif-sur-Yvette, 91191, France

10

11 Correspondence to: Nicolas Metzl (nicolas.metzl@locean.ipsl.fr)

12

13 **Keywords:** Acidification, Air-Sea CO₂ fluxes, Southern Ocean, Coastal, Adélie Land

14

15 **Abstract:**

16

17 Ocean acidification is expected to be particularly severe in Antarctic continental shelves due to
18 enhanced anthropogenic carbon uptake in cold waters in response to rising atmospheric CO₂, sea-ice
19 retreat, freshening and climate-change feedbacks. Models suggest that undersaturated conditions
20 with respect to aragonite (Ω_{ar}), a major form of calcium carbonate formed by marine species, could
21 be reached as soon as 2052 for austral winter. Here we present new ocean carbonate system
22 observations from cruises conducted since 2010 in the Adélie Land coastal region in East Antarctica,
23 along with data from a BCG-Argo float and results from a neural network model for the period 1985-
24 2025. The region is a permanent CO₂ sink and was most pronounced since 2006. The CO₂ sink leads
25 to a positive increase of surface water total CO₂ concentrations (C_T) ($+0.44 \pm 0.01 \mu\text{mol}\cdot\text{kg}^{-1}\cdot\text{yr}^{-1}$) and
26 to a progressive decrease of pH (-0.013 per decade) and Ω_{ar} (-0.035 per decade) for the winter
27 season. The lowest surface Ω_{ar} of 1.2 was observed in winter 2024 from the float data, a critical limit
28 for some marine species such as pteropod. A projection of the C_T concentrations in the future, based
29 on observed anthropogenic CO₂ concentrations and emissions scenarios, suggests that aragonite
30 saturation state ($\Omega_{ar} = 1$) will occur in surface waters as soon as 2055 in the Adélie Land region,
31 which is part of a larger area of East Antarctica proposed as a Marine Protected Area by the
32 Commission for the Conservation of Antarctic Marine Living Resources since the early 2010s.

33

34 **1 Introduction:**

35

36 Coastal and continental shelf waters can experience enhanced ocean acidification (OA) due
37 to increasing ocean CO₂ uptake in response to increased greenhouse forcing (Bourgeois et al 2016;
38 Laruelle et al, 2018; Roobaert et al, 2024a,b). As opposed to the offshore ocean, the detection of CO₂
39 and acidification trends in Antarctic coastal waters is complicated by multiple effects due to
40 anthropogenic CO₂ (C_{ant}) uptake, warming or cooling, variability in biological processes, upwelling,
41 and changes in sea-ice cover and freshening.

42 In the Southern Ocean, OA has been studied using sea surface CO₂ fugacity ($f\text{CO}_2$)
43 observations at regional scale mainly in the Sub-Antarctic, Polar Front or Permanent Open Ocean
44 zones (Xue et al 2018; Brandon et al 2022; Metzl et al 2024b). Apart from the Drake Passage to the
45 north of the Antarctic Peninsula (Takahashi et al, 2014; Hauri et al 2015; Munro et al, 2015) no long-
46 term time-series have been used to evaluate OA in coastal Antarctic zones. The observed pH rates at
47 Drake and Palmer station ranged between $+0.020 \pm 0.020$ and -0.015 ± 0.008 decade⁻¹. Recently,



48 Mazloff et al (2023) merged Biogeochemical Argo (BGC-Argo) float and historical observations to
49 estimate OA in the entire Southern Ocean (SO). In the seasonal ice zone (SIZ), they evaluated pH
50 trend of -0.0242 ± 0.0007 decade⁻¹ between 1994 and 2017 in subsurface waters (100-210m).
51 Estimates of the decadal change in OA based on observations, are often limited to data collected 2 to
52 15 years apart (e.g., Hauck et al., 2010; Pardo et al., 2017; Carter et al., 2019). In the regions of dense
53 water formation, C_{ant} is efficiently transported in the deep ocean implying that acidification can be
54 detected not only in surface waters but also in deep and bottom waters (Zhang et al, 2023). The
55 Adélie Land region is one of the four main bottom water formation regions in Antarctica with the
56 formation of Adélie Land Bottom Water (ALBW), which was first recognized by Gordon and Tchernia
57 (1972). Subsequently, a number of studies have described and quantified the variability of the ALBW
58 formation and its properties (e.g. Williams et al, 2010; Aoki et al, 2013; van Wijk and Rintoul 2014;
59 Schadwik et al, 2014; Pardo et al 2017). Once formed on the continental shelf and slope, ALBW is
60 transported away from its source, and ventilates the entire Australian-Antarctic Basin and beyond
61 (Sholeninova et al, 2025). As such, ALBW links the ocean CO₂ uptake in coastal waters, which have
62 been shown to be associated with significant C_{ant} concentrations of up to 44 $\mu\text{mol.kg}^{-1}$ in the shelf
63 waters (Shadwick et al, 2014), linking the ocean CO₂ uptake in coastal waters and OA at depth (Zhang
64 et al, 2023).

65 The Adélie Land is part of a proposed Marine Protected Area of East Antarctica (Boothroyd et
66 al, 2024) and severe undersaturated conditions with respect to aragonite could occur as soon as
67 2055 at the surface in austral winter and in 2080 for summer (Nissen et al, 2024). Preliminary results
68 based on summer observations gathered from 2002 to 2012 indicate that the trend of surface water
69 C_T in the Adélie Land region was not significant ($N-C_T$ trend = $+0.63 \pm 0.70$ $\mu\text{mol.kg}^{-1}.\text{yr}^{-1}$, Metzl et al
70 2025a). This region has large inter-annual variability in CO₂, linked to competitive processes between
71 anthropogenic CO₂ uptake, primary production, mixing, or ice melting (Shadwick et al., 2013, 2014,
72 2017) possibly masking the trend.

73 In this context, more data are needed to better evaluate the changes in the carbonate
74 system in Antarctic coastal zones and the associated OA (Tilbrook et al, 2019). This would allow us to
75 better evaluate the long-term changes with regard to the biological impacts and offer better
76 validation for ocean and Earth system models that struggle to reproduce the seasonal cycles of the
77 carbonate chemistry and remain poorly constrained to project future OA changes, particularly in high
78 latitudes.

79 In this study, we present new $f\text{CO}_2$ and C_T data obtained in January 2024 and in December-
80 February 2024-2025 in the Adélie Land region combined with historical data and machine learning
81 products to better define the seasonality and trends in CO₂ and OA. Using historical data since the
82 1980s and BGC-Argo float data in 2024-2025 we estimate the trends in the carbonate system (pH and
83 Ω_{ar}). As most observations were obtained in austral summer (December-March) the results from a
84 reconstruction of the global surface ocean carbonate system model (Chau et al, 2024) that extended
85 to 2025 were used to explore the decadal trends for different seasons. Based on subsurface
86 anthropogenic CO₂ concentrations estimates for 1995 to 2025 we investigate future changes in Ω_{ar} ,
87 that are predicted to reach undersaturation by the mid-century (Nissen et al, 2024), with potential
88 impact for marine species such as pteropods (e.g. Bednaršek et al, 2023).

89

90 **2 Data selection and methods**

91

92 **2.1 Data selection in the Adélie Land sector**



93

94 To explore the long-term change of the carbonate system in this region, we selected the $f\text{CO}_2$
95 data from Surface Ocean CO_2 Atlas (SOCAT), version v2025 (Bakker et al, 2016, 2025) with the
96 addition of 3 recent cruises conducted on-board the ship L'Astrolabe in December 2024, January
97 2025 and February 2025. These include 67 cruises from 1984 to 2025 south of 63°S and between
98 $140\text{--}150^\circ\text{E}$ (see the detail in Table S1 and Figure 1). During some cruises (MINERVE cruises between
99 2003 and 2012 and OISO-10 cruise in 2003) continuous underway or regular sampling for total
100 alkalinity (A_T) and C_T measurements were performed (data available in the SNAPO- CO_2 data-set,
101 Metzl et al, 2025a). During the L'Astrolabe cruise in January 2025, A_T and C_T samples in sea surface
102 water were also taken, analyzed at the SNAPO- CO_2 service facilities at LOCEAN laboratory
103 (Paris/France), and included in this work. In addition, we also used water column data between 1993
104 and 2018 from the Global Ocean Data Analysis Project (GLODAP), version GLODAPv2.2023 data-base
105 (Lauvset et al, 2023, 2024; Table S2); the GLODAP data in surface waters (0-30m) are also used to
106 synthesize all A_T and C_T data in the region and used to validate and compare results of the C_T and pH
107 trends based on $f\text{CO}_2$ data and to complement periods when $f\text{CO}_2$ data are not available. Finally, data
108 from a BGC-Argo float in 2024-2025 (WMO 2903867) are introduced to complement the water
109 column and winter data.

110

111 **2.2 Methods**

112

113 The methods to derive surface underway $f\text{CO}_2$ in SOCAT were described in previous studies
114 (e. g. Metzl et al, 1999; Ishii et al, 2002; Brévière et al, 2006; Laika et al, 2009; Midorikawa et al 2012;
115 Shadwick et al 2014 & 2017), or detailed in the cruises metadata of SOCAT. The methods for
116 underway or discrete A_T and C_T measurements were described and available in the SNAPO- CO_2 data-
117 set (Metzl et al, 2024a; 2025a). Here we describe the methods used during the L'Astrolabe 2024-
118 2025 cruise.

119

120 The underway $f\text{CO}_2$ measurements onboard L'Astrolabe in December 2024/February 2025
(Figure S1) were made by CSIRO, Hobart, using a General Oceanics 8050 $f\text{CO}_2$ system equipped with a
121 LICOR LI-7815 analyser (Pierrot et al, 2009; Tilbrook et al, 2025). The same technique was used
122 during Le Commandant Charcot voyage in 2023 and Investigator voyage in 2024. The precision of the
123 $f\text{CO}_2$ data are estimated to be $\pm 2 \mu\text{atm}$, with cruises flagged B in SOCAT (Table S1).

124

125 In January 2025, discrete sampling was performed from the ship's seawater supply for
126 salinity, A_T , C_T , $\delta^{13}\text{C}$, $\delta^{18}\text{O}$. For A_T and C_T samples were collected in 500 mL borosilicate glass bottles
127 and poisoned with 300 μL of HgCl_2 , closed with greased stoppers (Apiezon®) following the standard
128 operating procedures of Dickson et al. (2007). Discrete samples were returned to the LOCEAN
129 laboratory (Paris, France) in March 2025, stored in a dark room at 4°C , and analyzed in April 2025. A_T
130 and C_T were measured using a potentiometric titration method (Edmond, 1970) in a closed cell. For
131 calibration, we used the Certified Referenced Materials (CRM # 208) provided by Pr. A. Dickson (SIO,
132 University of California). A total of 31 samples were analyzed for the R2 cruise. Two anomalous
133 values were identified for both A_T and C_T either due to a sampling or analytical issues and were not
134 considered further (Supp. Mat. Figure S2). For the other data, we estimate that the accuracy for both
135 A_T and C_T is better than $4 \mu\text{mol.kg}^{-1}$, as for other samples measured at the SNAPO- CO_2 facilities
136 (Metzl et al, 2025a). These data were used for the validation of calculated carbonate system
parameters using $f\text{CO}_2$ data with an A_T /salinity relationship.



137 In this region a BGC-Argo float (WMO 2903867) was launched on 26 January 2024 at location
138 132°E/64°S and drifted south-eastward. Like other SOCCOM floats (Sarmiento et al, 2023) this float
139 recorded T, S, O₂, pH, Nitrates and Chl-a down to 1500m. The float data are available at
140 <https://www.mbari.org/products/data-repository/>, last access 10 May 2025). Its last record with
141 good pH data was on 15 January 2025 at 144.5°E/66.2°S. A_T was estimated with the LIAR V2.2
142 algorithm (Carter et al., 2016, 2017). From pH and A_T data we calculated C_T, Ω_{ar} and fCO₂ using the
143 same CO2sys code used for the shipboard data (section 2.3). Based on the uncertainty of the float
144 data and calculations the C_T, fCO₂ and Ω_{ar} errors are respectively of 6.8 μmol.kg⁻¹, 9.4 μatm and
145 0.103.

146

147 **2.3 Carbonate system calculation and A_T/Salinity relationship**

148

149 From fCO₂ or A_T and C_T data, we calculated pH_T (pH at total scale) and the saturation states of
150 aragonite and calcite (Ω_{ar}, Ω_{ca}). Here we used the CO2sys program (version CO2sys_v2.5, Orr et al.,
151 2018) with K₁ and K₂ dissociation constants from Lueker et al. (2000), KSO₄ dissociation constant from
152 Dickson (1990). Total boron concentration was calculated according to Uppström (1974). Nutrients
153 were not measured for many cruises and when not available we used fixed climatological values of
154 40 and 2 μmol.kg⁻¹ for silicate and phosphate respectively (Figure S3; Beucher et al, 2004; Bender et
155 al, 2016). When a strong bloom occurred, as indicated by high fluorescence and low fCO₂, the
156 nutrient concentrations were halved. The nutrient values used had no impact on the long-term
157 trends. When using fCO₂ data to derive pH_T, C_T, or Ω_{ar}, the A_T concentrations are derived from salinity
158 (e.g. Millero et al, 1998; Lee et al, 2006; Shadwick et al, 2014; Stark et al, 2018; Leseurre et al, 2022).
159 Here we used the A_T/Salinity relationship derived from A_T data in this region (Figure S4).

160

$$161 A_T (\mu\text{mol.kg}^{-1}) = 53.8059 (\pm 1.022) \times \text{Salinity} + 467.985 (\pm 34.600), (r^2 = 0.48, n = 2992) \quad (\text{Eq. 1})$$

162

163 This relation compared well with those previously estimated in the southern ocean (Lee et al
164 2006; Shadwick et al, 2014; Stark et al, 2018) as well as when derived from GLODAP data only (Figure
165 S4).

166

167 **2.4. CMEMS-LSCE-FFNN model and air-sea CO₂ fluxes**

168

169 We used the results from an ensemble of feed-forward neural networks (CMEMS-LSCE-FFNN
170 or FFNN for simplicity, Chau et al, 2024) to estimate fCO₂, A_T and C_T for seasons when direct
171 observations were not available. The FFNN model composes monthly surface ocean global fields of
172 surface ocean fCO₂ at 0.25°x0.25° resolution based on the SOCAT gridded data. The reconstructed
173 fCO₂ field for 1985-2025 was used to derive air-sea CO₂ fluxes, as well as together with A_T obtained
174 by a multi-linear regression approach, monthly surface C_T, pH_T and aragonite and calcite saturation
175 states. The FFNN dataset, including uncertainty estimates, are available under the DOI
176 <https://doi.org/10.48670/moi-00047>. We used the results in the region 65-66.5°S/139-141°E.

177

178 During the first period, 1985-2000, the FFNN model estimated a CO₂ flux close to 0 (average =
179 -0.030 ± 0.107 molC.m⁻².yr⁻¹). After 2000, the model suggests an increase of the CO₂ sink especially
180 after 2016 (Figure 2), a signal identified at a larger scale in the Antarctic Seasonal Ice Zone in Spring-
181 Summer 2003-2022 (Deng et al, 2025). The maximum CO₂ sink of -1.2 molC.m⁻².yr⁻¹ occurred in 2023.
181 This is much stronger than the flux of -0.31 molC.m⁻².yr⁻¹ derived from the climatology in 2010 (Fay et



182 al, 2024). In austral summer, the variability of the flux could be large. Previous studies reported
183 fluxes ranging between +0.1 to -3.5 mmolC.m⁻².d⁻¹ in summer in this region (Ishii et al, 2002; Arroyo
184 et al 2020) but the CO₂ sink could be up to -15 to -30 mmolC.m⁻².d⁻¹ in the Mertz Polynya region east
185 of the Adélie Land (Schadwik et al 2014; 2017). In January 2023 the sink derived from the FFNN
186 model reached a maximum of -17 mmolC.m⁻².d⁻¹. This was associated to low fCO₂ (321.5 µatm) and
187 high wind speed (up to 7.8 m.s⁻¹) during a high positive Southern Annual Mode (SAM index of 4.56 in
188 January 2023). Strong CO₂ sinks, < -10 mmolC.m⁻².d⁻¹, were also estimated in January 2019 and in
189 February 2002, 2016 and 2021 also associated to positive SAM (>1.4). In January and February 2025,
190 the period of the Astrolabe cruises, the sink was respectively -7.6 ±2.9 and -12.1 ±6.1 mmolC.m⁻².d⁻¹
191 (when the SAM was respectively only 1.4 and 0.31). The impact of the CO₂ uptake and its increase
192 over time on the pH_T and Ω_{ar} changes is discussed in the following sections.

193

194 **3 Results and discussion**

195

196 **3.1 Recent cruises and a BGC-Argo float (2024-2025)**

197

198 **3.1.1 Distribution in 2024-2025**

199

200 The 2024-2025 shipboard and BGC-Argo observations consistently showed the ocean was a
201 CO₂ sink in summer (Figure 3). The large spatial variability observed at 66-67°S, with fCO₂ lower than
202 300 µatm, was linked to biological activity concentrated near the coast above the Adélie Bank (140-
203 142°E) and the Mertz Bank (145-147°E) (Figure S5). Biological processes also drove significant inter-
204 annual changes. For example, along the ~140°E track visited in January 2024 (RV/Investigator) and in
205 February 2025 (L'Astrolabe), fCO₂ showed the same southward decrease but shifted by 26 µatm,
206 while only 7 µatm is attributable to the temperature differences (Figure 4a). The C_T concentrations
207 derived from the fCO₂ data indicated that the difference was most pronounced at 65.3°S (Figure 4b)
208 where the Chl-a was higher in 2024 (Figure S5). This demonstrates that biology drives most spatial
209 and temporal variability making C_T or pH_T trend detection difficult in Antarctic coastal summer data
210 (Metzl et al, 2025a).

211 A BGC-Argo float (WMO 2903867) provided wintertime fCO₂ data for 2024 (Figure 5). The
212 maximum fCO₂ of 440 µatm, above the atmospheric CO₂ level, occurred in September (Figure 5a). In
213 September 2024, and given the error associated to the fCO₂ data derived from the float (±9.4 µatm),
214 we estimated a positive ocean-atmosphere difference (ΔfCO₂ > 0, a potential CO₂ source) with a
215 range between 28.4 and 9.6 µatm. In August 1996 during the only cruise conducted in austral winter
216 (Exocode 09AR19960822) we estimated fCO₂ from the A_T C_T data in surface waters. This also led to
217 a potential CO₂ source, ΔfCO₂ ranging between 31.7 and 7.5 µatm. For the same periods, August
218 1996 and September 2024, ΔfCO₂ from the FFNN model were respectively 37.95 and 12.4 µatm. The
219 air-sea CO₂ fluxes estimated by the FFNN model were +0.176 mmol C.m⁻².d⁻¹ in August 1996 and +
220 0.184 mmol C.m⁻².d⁻¹ in September 2024, i.e. a similar value observed 28 years apart.

221 In September 2024 the sea surface C_T estimate from the float reached a maximum of 2221.3
222 ±1.9 µmol.kg⁻¹ compared to 2207.2 ±3.7 µmol.kg⁻¹ measured in August 1996 (Figure 5b). The
223 difference of +14.1 µmol.kg⁻¹ would translate into a rate of +0.5 µmol.kg⁻¹.yr⁻¹ over 28 years similar to
224 the range of the anthropogenic CO₂ trend in the Antarctic Surface Water (AASW), +0.35 ±0.14 to
225 +0.65 ±0.21 µmol.kg⁻¹.yr⁻¹ derived from 4 cruises in 1995-2011 in this region (Pardo et al, 2017).
226 Consequently, pH_T decreased from 8.054 ±0.005 (winter 1996) to 7.976 ±0.002 (winter 2024) (Figure



227 5c) and Ω_{ar} decreased from 1.334 ± 0.017 to 1.157 ± 0.009 (Figure 5d). A pH_T decrease of 0.0781 in 28
228 years corresponds to a trend of -0.028 per decade. This substantial signal derived from measured pH
229 (BGC-Argo in 2024) and calculated pH_T (shipboard A_T and C_T data in 1996), is sensitive to method
230 uncertainties. Accounting for A_T and C_T measurements uncertainty ($\pm 4 \mu\text{mol.kg}^{-1}$, Lauvset et al, 2024)
231 the pH_T decrease ranges from -0.021 to -0.035 per decade consistent with previous estimates of -
232 0.035 ± 0.002 per decade in the AASW in this region (Pardo et al, 2017). This rapid pH_T decrease
233 requires confirmation with longer time series and quantification of contributing processes
234 (anthropogenic CO_2 signal, mixing, warm deep water intrusion, sea-ice extent, natural variability...).

235

236 **3.1.2 The period 1985-2025: high variability in summer, trends in winter**

237

238 To evaluate trends we averaged data from each cruise around 140°E and south of 65°S . In
239 this region $f\text{CO}_2$ data from SOCAT are available since 1984 and A_T and C_T data from GLODAP and
240 SNAPO- CO_2 since 1994. The FFNN model starts in 1985 and was constrained by satellite Chl-a data
241 since 1998, and by climatological Chl-a before then.

242 The average $f\text{CO}_2$ and C_T data present higher values in recent years (Figure 6). The $f\text{CO}_2$
243 average for January 2025 (mean = $382.3 \mu\text{atm}$) was much higher than the first data in January 1984
244 ($f\text{CO}_2 = 317.5 \mu\text{atm}$). The difference of $64.8 \mu\text{atm}$ would translate into a trend of $+1.58 \mu\text{atm.yr}^{-1}$ with
245 the atmospheric trend of $+1.98 \text{ppm.yr}^{-1}$ for the same period. In January 2025, the C_T measurements
246 (C_T normalized at salinity 34, $N-C_T = 2182 \mu\text{mol.kg}^{-1}$) increased by $+10 \mu\text{mol.kg}^{-1}$ compared to January
247 1994 ($N-C_T = 2172 \mu\text{mol.kg}^{-1}$) corresponding to a trend of $+0.32 \mu\text{mol.kg}^{-1.yr}^{-1}$.

248 Although the C_T data present higher concentrations in the recent decade, the trends based
249 on observations are uncertain due to the large inter-annual variability (Table 1). Indeed, the time
250 series of $f\text{CO}_2$ and C_T present large inter-annual variability in summer (Figure 6) which is particularly
251 apparent in 2002 and 2015 and was clearly linked to biological activity (Figure S6). The FFNN model
252 captured these anomalies leading to stronger CO_2 sinks in summer 2002 and 2015 (Figure 2, Figure
253 S7). This also led to anomalies in pH_T and Ω_{ar} (Figure 7). Consequently, the long-term trends of
254 observed properties in summer are uncertain and the errors associated with the trends in the FFNN
255 model are also larger in summer compared to winter (Table 1). A simple linear projection of the Ω_{ar}
256 trend in winter from the FFNN model ($-0.0035 \pm 0.0001 .\text{yr}^{-1}$) suggests that a value of 1.2 would be
257 reached in 2032 and saturation ($\Omega_{ar}=1$) in 2090.

258 The observations indicate that the lowest Ω_{ar} occurred in winter 2024 (BGC-Argo data, $\Omega_{ar} =$
259 1.146, on 6 September 2024). This is 0.25 lower than in 1985 and 0.15 lower than in 1996 and the
260 decrease of Ω_{ar} in surface also occurred at depth (Figure 8). In the mixed layer Ω_{ar} decreased from
261 around 1.35 in August 1996 to 1.15 in winter 2024. Such a value is observed at 200m in January 2025
262 and at 300-400m in 1996 indicating an upward migration of Ω_{ar} (Pardo et al, 2017). We noticed that
263 the FFNN value in August 1996 ($\Omega_{ar} = 1.34$) was coherent with that observed in August 1996 in the
264 mixed-layer (Figure 8). In August 2024 and 2025, the FFNN value ($\Omega_{ar} = 1.23$) is close to that observed
265 from the float in winter 2024 ($\Omega_{ar} = 1.2$) and to the data observed at 200 m in 1996 or at 75 m in
266 2025. The distribution of Ω_{ar} for the FFNN is more homogeneous in winter (Figure S8) and provides a
267 smaller error estimate of the long term trend but is constrained by few observations. The FFNN
268 model also has a more variable air-sea CO_2 flux during summer compared to winter (Figure S9),
269 leading to significant change in annual CO_2 uptake (Figure 2). The seasonal amplitude from the FFNN
270 results also show significant variability over 5-10 years after 1998 (Figure S10) but no trend of the
271 $f\text{CO}_2$ seasonality was detected as was suggested in other ocean regions (e.g. Landschützer et al.,



272 2018; Rodgers et al., 2023; Shadwick et al 2023). To estimate the processes that drive the pH_T and
273 Ω_{ar} changes we focus on results for the winter season.

274

275 **3.1.3 Anthropogenic CO₂**

276

277 To estimate the anthropogenic CO₂ concentrations (C_{ant}) in the water column we used the
278 TrOCA method developed by Touratier et al. (2007). This method was successfully used in the
279 southern Indian Ocean (Shadwick et al, 2014; Mahieu et al., 2020; Zhang et al, 2023; Metzl et al,
280 2024b). Here we selected the data below 100m depth for 1994-2018 and from the BGC-Argo float
281 (March 2024 to January 2025, Figure S11). The C_{ant} trends were tested in three layers, 100-150 m,
282 150-200 m and 200-250 m (Figure 9). In all layers, the mean C_{ant} concentration ranged from 15-25
283 $\mu\text{mol.kg}^{-1}$ in 1995-1996 to 30-35 $\mu\text{mol.kg}^{-1}$ in 2024. C_T and C_{ant} concentrations present positive trends
284 (Table 2, Figure 9a and Figure S12). No significant changes were observed for A_T (not shown) but we
285 noticed that $\delta^{13}\text{C}$ observations in January 2025 were lower than in January 2003 suggesting that
286 surface waters captured the anthropogenic Suess effect signal (Figure S13) as previously observed in
287 this region (McNeil et al, 2001). Without the BGC-Argo data the C_{ant} trend would be $+0.50 \pm 0.20$
288 $\mu\text{mol.kg}^{-1}.\text{yr}^{-1}$. This is almost the same as derived for surface C_T in winter from the FFNN model
289 ($0.44 \pm 0.01 \mu\text{mol.kg}^{-1}.\text{yr}^{-1}$) and equal to the trend derived from only two winter observations (Table
290 1). The anthropogenic subsurface CO₂ signal was also present in the winter surface data, but these
291 are based on only two observational periods. Our results are similar to previous C_{ant} trend estimates
292 for the region, ranging between $+0.35$ and $+0.65 \mu\text{mol.kg}^{-1}.\text{yr}^{-1}$ (Pardo et al, 2017). In 2013 low C_{ant}
293 concentrations were estimated in the three layers and were associated with higher temperature,
294 salinity, nitrate and C_T , and lower O₂ concentrations (Figure S12) probably linked to regional import
295 of warmer Upper Circumpolar Deep Water (UCDW) that contains high C_T , low O₂ and low C_{ant} (e.g.
296 Shadwick et al, 2014; Pardo et al, 2017). The FFNN model produced slightly higher surface C_T
297 concentrations in 2013 ($+6 \mu\text{mol.kg}^{-1}$, Figure 9a, S12d). This 2013 anomaly has very little impact on
298 the estimated trend; removing 2013 yields a trend of $+0.42 \mu\text{mol.kg}^{-1}.\text{yr}^{-1}$ compared to $+0.37 \mu\text{mol.kg}^{-1}.$
299 yr^{-1} for the whole time series (Table 2). To quantify the impact of C_{ant} on the C_T , pH_T and Ω_{ar} trends
300 in surface waters, we used both estimates (with or without 2013 data for sensitivity analysis). For the
301 layer 100-150 m, the relationship of C_{ant} versus atmospheric CO₂ concentration, XCO_2 (Figure 9b) are
302 as follow:

303

304 All years: $C_{ant} = 0.179 (\pm 0.081) \times XCO_2 - 38.5 (\pm 31.1)$; $r_2 = 0.41$ (Eq. 2)

305 Without 2013: $C_{ant} = 0.190 (\pm 0.071) \times XCO_2 - 41.6 (\pm 27.2)$; $r_2 = 0.54$ (Eq. 3)

306 Without 2024: $C_{ant} = 0.197 (\pm 0.118) \times XCO_2 - 45.1 (\pm 44.7)$; $r_2 = 0.32$ (Eq. 4)

307

308 These equations are used to compare the time-series and project the trend in the future.

309

310 **3.4 Carbonate system reconstruction and projection in the future**

311

312 To reconstruct the temporal change of the carbonate system properties (Metzl et al, 2025b) we used
313 the relations between C_{ant} and atmospheric CO₂ described above and calculated the C_T concentration
314 each year correcting C_T as follows, where t represents the time-step in year, from 1960 to 2100:

315

316 $C_T(t) = C_T(t-1) + C_{ant}(t) - C_{ant}(t-1)$ (Eq. 5)



317

318 The values of X_{CO_2} in equation 2, 3 or 4 were derived from SSP emissions scenarios (Shared
319 Socioeconomic Pathways, Meinshausen et al., 2020). We selected a “high” emission scenario SSP5-
320 8.5 and a stabilization scenario SSP2-4.5 and we applied Equation 5 for August using either the C_{ant}
321 trend (Table 2) or Eq. 2 (Eq. 3 or Eq 4 were tested but led to the same results). Temperature, salinity
322 and alkalinity were fixed ($SST = -1.8$ °C; $SSS = 34.2$; $A_T = 2310$ $\mu\text{mol.kg}^{-1}$) and f_{CO_2} , pH_T and Ω_{ar} were
323 calculated using version CO2sys_v2.5 (Orr et al, 2018).

324 The estimated C_T using the C_{ant} trend (Eq. 5) is close to the FFNN model and observations
325 (Figure 10a). The mean difference of C_T for all years (1985-2025) is -1.72 ± 1.53 $\mu\text{mol.kg}^{-1}$. This
326 suggests that anthropogenic CO_2 is a main driver of C_T changes but other process could explain the
327 full trend in surface C_T . In 2009 and 2013 the difference is larger than 4 $\mu\text{mol.kg}^{-1}$ (Figure S14). As
328 discussed above, the import of warm and rich- C_T UCDW in 2013 likely increased the surface C_T . For
329 2009 there was no data in the water column to explore such scenario but the same process may have
330 occurred.

331 Based on this estimation, we conclude that the anthropogenic CO_2 uptake represents 70% of
332 the C_T increase over 1985-2025. This also drives the decrease of pH_T and Ω_{ar} (Figures 10 c,d).
333 Projecting the trends from the FFNN model and the reconstruction, a value of 1.2 for Ω_{ar} would be
334 reached in year 2032 from the FFNN model against 2034 for the estimation based on Eq. 5. If correct,
335 this would lead to “severe shell dissolution” for pteropods (Bednaršek et al, 2019).

336 In the Adélie Land region the aragonite saturation depth (ASD, $\Omega_{ar} = 1$) was observed at 1000
337 m in 1995 and at 700 m in 2011 (Pardo et al, 2017). In summer 2007/2008, Shadwick et al (2014) also
338 reported an ASD around 700-900 m. The data in 2018 and 2024 also identified the ASD at 800-1000
339 m but Ω_{ar} values close to 1 were also observed at 100m (Figure 11). At around 100-200m depth, this
340 is probably linked to remineralized C_T in the remnant winter layer, leading to homogeneous and low
341 Ω_{ar} (1.15) after mixing/upwelling in wintertime (Figure 8).

342 We are now interested in exploring when the aragonite undersaturation would be reached in
343 surface waters (Figure 12). The sensitivity analysis based on the two C_{ant}/CO_2 relationships (Eq. 2 and
344 Eq. 3) show the same results. For the future, differences between the two scenarios (SSP5-8.5 and
345 SSP2-4.5) are large after 2040 (Table 3). For the high scenario, the surface C_T concentrations reaches
346 2250 $\mu\text{mol.kg}^{-1}$ in 2060, a concentration observed in the Adélie Land Bottom Water (ALBW)
347 (Shadwick et al 2014). After 2060, pH_T is lower than 7.9. Based on the high scenario, the aragonite
348 undersaturation would be reached in 2055 (at atmospheric $CO_2 = 600$ ppm). This is much sooner than
349 deduced in the Southern Ocean from the Coupled Model Intercomparison Project Phase 6 (CMIP6)
350 global models ($\Omega_{ar} = 1.04$ in 2080, Table S9 in Jiang et al, 2023) and would have potential dramatic
351 impact on species such as pteropods (Bednaršek et al, 2012; 2023) as well as for diatoms abundant in
352 the SO (e.g. Petrou et al., 2019; Duncan et al., 2022).

353 In our projection, the C_{ant} concentration of 25 $\mu\text{mol.kg}^{-1}$ in 1990 reached 140.5 $\mu\text{mol.kg}^{-1}$ in
354 2090 for the scenario SSP5-8.5. In 2090, a pH_T of 7.67 and an Ω_{ar} of 0.581 are in line with the results
355 of a high-resolution ocean model in the East Antarctica region (a proposed Marine Protected Area,
356 Nissen et al, 2024). Their model suggested that aragonite undersaturation would occur in 2050,
357 coherent with our projection (2055, Figure 12). For a low emission scenario (SSP2-4.5) this would not
358 occur before 2080 (Figure 12).

359

360 **4. Summary and concluding remarks**

361



362 New $f\text{CO}_2$, C_T , A_T shipboard and pH_T BGC-Argo observations in 2024 and 2025 and historical
363 $f\text{CO}_2$ data available since 1984 were used to evaluate the decadal trends of the carbonate system in
364 the Adélie Land region.

365 The sea surface C_T and $f\text{CO}_2$ measurement in summer 2024-2025 present very high variability
366 linked to biological activity. The mean measured $f\text{CO}_2$ observation in January 2025 of $382.3 \mu\text{atm}$ was
367 much higher than in January 1984 ($f\text{CO}_2 = 317.5 \mu\text{atm}$) but in February 2025 $f\text{CO}_2$ decreased to 317.8
368 $\pm 33.8 \mu\text{atm}$ close to $f\text{CO}_2$ derived from the BGC-Argo float in January 2025 ($311.6 \pm 12.2 \mu\text{atm}$).
369 Previous $f\text{CO}_2$ observations ranged from $179.2 \mu\text{atm}$ in 2002 to $376.7 \mu\text{atm}$ in 2007, highlighting the
370 large inter-annual variability in summer.

371 In summer 2025, the measured C_T between 2130 and $2190 \mu\text{mol.kg}^{-1}$ were much lower than
372 C_T derived from the BGC-Argo data in winter 2024 ($2221 \mu\text{mol.kg}^{-1}$) whereas in winter 1996, the
373 measured C_T was $2207 \mu\text{mol.kg}^{-1}$. The winter C_T increase from 1996 to 2024 translates into a signal of
374 anthropogenic CO_2 uptake. Using an adapted A_T/S relationship for this region, pH_T and Ω_{ar} were
375 calculated from C_T or $f\text{CO}_2$ data. We estimated a pH_T decrease in surface waters from 8.054 ± 0.005 in
376 winter 1996 (calculated from shipboard data) to 7.976 ± 0.002 in winter 2024 (measured from the
377 BGC-Argo float). The calculated Ω_{ar} decreased from 1.334 ± 0.017 in 1996 to 1.157 ± 0.009 in 2024.

378 As most data were available in summer, the results of a monthly FFNN model were used to
379 estimate the long-term trends. The FFNN model informed that the region was a permanent CO_2 sink
380 and most pronounced since 2006. The maximum sink occurred in 2023 ($-1.2 \text{ molC.m}^{-2}.\text{yr}^{-1}$) when the
381 SAM was positive. Results from the FFNN model indicate a pH_T decrease of -0.013 per decade and Ω_{ar}
382 decrease of -0.035 per decade over 1985-2025 in winters. As no change in alkalinity was observed,
383 the OA was mainly explained by the C_T increase ($0.44 \pm 0.01 \mu\text{mol.kg}^{-1}.\text{yr}^{-1}$) associated with
384 accumulation of anthropogenic CO_2 calculated from subsurface data since 1995.

385 A projection of the C_T concentrations in the future, based on observed anthropogenic CO_2
386 concentrations and emissions scenarios, suggests that aragonite undersaturation would occur in
387 surface water as soon as 2055 with potential impacts on plankton species such as pteropods (and
388 many others species). Interestingly, our data-based analysis is in line with the results of a high-
389 resolution ocean model dedicated to the Marine Protected Areas in the Antarctic coastal zone
390 (Nissen et al, 2024). Their model suggests that climate-change feedbacks, through warming, sea-ice
391 extend, or upwelling, might accelerate OA in these regions. Our simple projection (Figure 12) does
392 not take into account effects of warming, cooling, change of upwelling with rich- C_T waters, or
393 freshening. As opposed to other oceanic regions (Cheng et al, 2025), the Adélie Land coastal region
394 experienced a surface cooling trend of between -0.1 to -0.3°C per decade in surface water (Auger et
395 al., 2021, for summer 1993-2017). For the period 1993-2023, Morrow and Kestenare (2025) also
396 estimate a cooling of -0.06°C per decade and a freshening of -0.012 per decade. Such a cooling and
397 freshening would increase pH_T by only $+0.00897$ and reduce Ω_{ar} by -0.00112 in 2100 representing a
398 small change compared to the effect of CO_2 emissions. The results presented here support
399 maintaining observations in the Adélie Land region, both from shipboard and BGC-Argo floats, and to
400 investigate property changes and OA in other Antarctic coastal zones.

401

402 **Acknowledgments:**

403

404 The Astrolabe data since 1996 were collected as part of a French-Australia collaboration. Underway
405 $f\text{CO}_2$ data from Astrolabe 2024-2025 and earlier Australian cruises were sourced from CSIRO and
406 Australia's Integrated Marine Observing System (IMOS) – IMOS is enabled by the National



407 Collaborative Research Infrastructure Strategy (NCRIS). The OISO program on-board Marion-Dufresne
408 was supported by the French institutes INSU (Institut National des Sciences de l'Univers) and IPEV
409 (Institut Polaire Paul-Emile Victor), OSU Ecce-Terra (at Sorbonne Université). We also acknowledge
410 INSU/CNRS and OSU ECCE-Terra for supporting the SNAPO-CO2 facility housed by the LOCEAN
411 laboratory in Paris/France. The development of the neural network model benefited from funding by
412 the French INSU-GMMC project "PPR-Green-Grog (grant no 5-DS-PPR-GGREOG), the EU H2020
413 project AtlantOS (grant no 633211), as well as through the Copernicus Marine Environment
414 Monitoring Service (project 83-CMEMS-TAC-MOB). MG was funded by the European Union under
415 grant agreement no. 101083922 (OceanICU). Views and opinions expressed are however those of the
416 author(s) only and do not necessarily reflect those of the European Union or European Research
417 Executive Agency. Neither the European Union nor the granting authority can be held responsible for
418 them. The Surface Ocean CO2 Atlas (SOCAT, www.socat.info) is an international effort, endorsed by
419 the International Ocean Carbon Coordination Project (IOCCP) and the Surface Ocean Lower
420 Atmosphere Study (SOLAS) to deliver a uniformly quality-controlled surface ocean CO2 database. We
421 thank François Forget, Rafik Hassen-Khodja and Ehouarn Millour for discrete sampling during 2025
422 Astrolabe cruises. Rik Wanninkhof provided comments on a preliminary draft.

423

424 **Authors contributions:**

425 CLM and NM are co-investigators of the ongoing Océan Indien Service d'Observation (OISO) project.
426 JBS is principal investigator of the Sustained Observation of the Southern Ocean (SOSO) project. BT,
427 JA and CN provided the $f\text{CO}_2$ data, AA analyzed the A_T C_T data and GR provided the C13 data from
428 L'Astrolabe cruises in 2024-2025. NM provided the A_T C_T data from SNAPO-CO2 database. MG and FC
429 developed the CMEMS-LSCE-FFNN model and AB provided the model results. NM started the
430 analysis, wrote the draft of the manuscript and prepared the figures with contributions from all co-
431 authors.

432

433 **Data availability:**

434 Data used in this study are available in SOCAT (Bakker et al, 2016, www.socat.info) for $f\text{CO}_2$ surface
435 data, and in GLODAP (Lauvset et al, 2023, 2024, www.glodap.info) for water-column data. The A_T and
436 C_T underway data from OISO and MINERVE cruises are available in Seanoe (Metzl et al, 2024a,
437 <https://www.seanoe.org>, <https://doi.org/10.17882/102337>). The BGC-Argo float data with derived
438 carbon parameters are available from SOCCOM (<https://socom.org>,
439 <https://www.mbari.org/products/data-repository/>). The CMEMS-LSCE-FFNN model data are
440 available at E.U. Copernicus Marine Service Information
441 (<https://resources.marine.copernicus.eu/products>, <https://doi.org/10.48670/moi-00047>).

442

443 **References**

444

445 Aoki, S., Y. Kitade, K. Shimada, K. I. Ohshima, T. Tamura, C. C. Bajish, M. Moteki, and S. R. Rintoul
446 (2013), Widespread freshening in the Seasonal Ice Zone near 140E off the Adelie Land Coast,
447 Antarctica, from 1994 to 2012, *J. Geophys. Res. Oceans*, 118, 6046–6063,
448 doi:10.1002/2013JC009009.

449



450 Arroyo, M. C., Shadwick, E. H., Tilbrook, B., Rintoul, S. R., & Kusahara, K. (2020). A continental shelf
451 pump for CO₂ on the Adélie Land coast, East Antarctica. *Journal of Geophysical Research: Oceans*,
452 125, e2020JC016302. <https://doi.org/10.1029/2020JC016302>
453

454 Auger, M., Morrow, R., Kestenare, E., Sallée, J.-B., and Cowley, R.: Southern Ocean in-situ
455 temperature trends over 25 years emerge from interannual variability, *Nat. Commun.*, 12, 514,
456 <https://doi.org/10.1038/s41467-020-20781-1>, 2021
457

458 Bakker, D. C. E., Pfeil, B., Landa, C. S., Metzl, N., O'Brien, K. M., Olsen, A., Smith, K., Cosca, C.,
459 Harasawa, S., Jones, S. D., Nakaoka, S.-I., Nojiri, Y., Schuster, U., Steinhoff, T., Sweeney, C., Takahashi,
460 T., Tilbrook, B., Wada, C., Wanninkhof, R., Alin, S. R., Balestrini, C. F., Barbero, L., Bates, N. R., Bianchi,
461 A. A., Bonou, F., Boutin, J., Bozec, Y., Burger, E. F., Cai, W.-J., Castle, R. D., Chen, L., Chierici, M.,
462 Currie, K., Evans, W., Featherstone, C., Feely, R. A., Fransson, A., Goyet, C., Greenwood, N., Gregor, L.,
463 Hankin, S., Hardman-Mountford, N. J., Harlay, J., Hauck, J., Hoppema, M., Humphreys, M. P., Hunt, C.
464 W., Huss, B., Ibánhez, J. S. P., Johannessen, T., Keeling, R., Kitidis, V., Körtzinger, A., Kozyr, A.,
465 Krasakopoulou, E., Kuwata, A., Landschützer, P., Lauvset, S. K., Lefèvre, N., Lo Monaco, C., Manke, A.,
466 Mathis, J. T., Merlivat, L., Millero, F. J., Monteiro, P. M. S., Munro, D. R., Murata, A., Newberger, T.,
467 Omar, A. M., Ono, T., Paterson, K., Pearce, D., Pierrot, D., Robbins, L. L., Saito, S., Salisbury, J.,
468 Schlitzer, R., Schneider, B., Schweitzer, R., Sieger, R., Skjelvan, I., Sullivan, K. F., Sutherland, S. C.,
469 Sutton, A. J., Tadokoro, K., Telszewski, M., Tuma, M., Van Heuven, S. M. A. C., Vandemark, D., Ward,
470 B., Watson, A. J., Xu, S., 2016. A multi-decade record of high-quality fCO₂ data in version 3 of the
471 Surface Ocean CO₂ Atlas (SOCAT), *Earth Syst. Sci. Data*, 8, 383-413, doi:10.5194/essd-8-383-2016.
472

473 Bakker, Dorothee C. E.; Alin, Simone R.; Aramaki, Takafumi; Barbero, Leticia; Bates, Nicholas;
474 Gkritzalis, Thanos; Jones, Steve D.; Kozyr, Alex; Lauvset, Siv K.; Macovei, Vlad A.; Metzl, Nicolas;
475 Munro, David R.; Nakaoka, Shin-ichiro; O'Brien, Kevin M.; Olsen, Are; Pierrot, Denis; Steinhoff,
476 Tobias; Sullivan, Kevin F.; Sutton, Adrienne J.; Sweeney, Colm; Wada, Chisato; Wanninkhof, Rik; Akl,
477 John; Arbillá, Lisandro A.; Azetsu-Scott, Kumiko; Battisti, Roman; Beatty, Cory M.; Becker, Meike;
478 Benoit-Cattin, Alice; Berghoff, Carla F.; Bittig, Henry C.; Bonin, Jennifer A.; Bott, Randy; Bozzano,
479 Roberto; Burger, Eugene F.; Brunetti, Fabio; Cantoni, Carolina; Castelli, Giuliano; Chambers, Don P.;
480 Chierici, Melissa; Corbo, Andrea; Cronin, Margot; Cross, Jessica N.; Currie, Kim I.; Dentico, Carlotta;
481 Emerson, Steven R.; Enochs, Ian C.; Enright, Matt P.; Enyo, Kazutaka; Ericson, Ylva; Evans, Wiley; Fay,
482 Amanda R.; Feely, Richard A.; Fragiaco, Elena; Fransson, Agneta; Gehrung, Martina; Giani,
483 Michele; Glockzin, Michael; Hamna, Siyabulela; Holodkov, Nikola; Hoppema, Mario; Ibánhez, J.
484 Severino P.; Kadono, Koji; Kamb, Linus; Kralj, Martina; Kristensin, Tor O.; Laudicella, V. Alessandro;
485 Lefèvre, Nathalie; Leseurre, Coraline; Lo Monaco, Claire; Maenner Jones, Stacy; Maenza, Reinaldo A.;
486 McAuliffe, Anna M.; Mdokwana, Baxolele; Monacci, Natalie M.; Musielewicz, Sylvia; Neill, Craig;
487 Newberger, Tim; Nojiri, Yukihiko; Ohman, Mark D.; Ólafsdóttir, Sólveig R.; Olivier, Léa; Omar,
488 Abdirahman M.; Osborne, John; Pensieri, Sara; Petersen, Wilhelm; Plueddemann, Albert J.; Rehder,
489 Gregor; Roden, Nicholas P.; Rutgersson, Anna; Sallée, Jean-Baptiste; Sanders, Richard; Sarpe, Dick;
490 Schirnik, Carsten; Schlitzer, Reiner; Send, Uwe; Skjelvan, Ingunn; Sutherland, Stewart, C.; T'Jampens,
491 Michiel; Tamsitt, Veronica; Telszewski, Maciej; Theetaert, Hannelore; Tilbrook, Bronte; Trull, Tom;
492 Tsanwani, Mutshutshu; Van de Velde, Sebastiaan; Van Heuven, Steven M. A. C.; Vecchia, Martín H.;
493 Voynova, Yoana G.; Weller, Robert A.; Williams, Nancy L. (2025). Surface Ocean CO₂ Atlas Database
494 Version 2025 (SOCATv2025) (NCEI Accession 0304549). [indicate subset used]. NOAA National



- 495 Centers for Environmental Information. Unpublished Dataset. <https://doi.org/10.25921/648f-fv35>.
496 Last Access 5 June 2025.
497
- 498 Barrett, R. C., Carter, B. R., Fassbender, A. J., Tilbrook, B., Woosley, R. J., Azetsu-Scott, K., et al.
499 (2025). Biological responses to ocean acidification are changing the global ocean carbon cycle. *Global*
500 *Biogeochemical Cycles*, 39, e2024GB008358. <https://doi.org/10.1029/2024GB008358>
501
- 502 Bednaršek, N. et al. Extensive dissolution of live pteropods in the Southern Ocean. *Nat. Geosci.* 5,
503 881–885, 2012.
504
- 505 Bednaršek, N., R. A. Feely, E. L. Howes, et al. 2019. “Systematic Review and Meta-Analysis Toward
506 Synthesis of Thresholds of Ocean Acidification Impacts on Calcifying Pteropods and Interactions With
507 Warming.” *Frontiers in Marine Science* 6: 227. <https://doi.org/10.3389/fmars.2019.00227>.
508
- 509 Bednaršek, N., R.A. Feely, G. Pelletier, and F. Desmet. 2023. Global synthesis of the status and trends
510 of ocean acidification impacts on shelled pteropods. *Oceanography* 36(2–3):130–137,
511 <https://doi.org/10.5670/oceanog.2023.210>
512
- 513 Bender, M. L., Tilbrook, B., Cassar, N., Jonsson, B., Poisson, A., and Trull, T. W.: Ocean productivity
514 south of Australia during spring and summer, *Deep Sea Research Part I: Oceanographic Research*
515 *Papers*, Volume 112, Pages 68-78, <https://doi.org/10.1016/j.dsr.2016.02.018>, 2016
516
- 517 Beucher, C., P. Tréguer, A.-M. Hapette, R. Corvaisier, N. Metzl, and J.-J. Pichon (2004), Intense
518 summer Si-recycling in the surface Southern Ocean, *Geophys. Res. Lett.*, 31, L09305,
519 doi:10.1029/2003GL018998.
520
- 521 Boothroyd, A., Adams, V., Alexander, K., & Hill, N.: Stakeholder perceptions of the Commission for
522 the Conservation of Antarctic Marine Living Resources Marine Protected Area planning process.
523 *Marine Policy*, 170, Article 106381. <https://doi.org/10.1016/j.marpol.2024.106381>, 2024.
524
- 525 Bourgeois, T., J. C. Orr, L. Resplandy, J. Terhaar, C. Ethé, M. Gehlen, and L. Bopp: Coastal-ocean
526 uptake of anthropogenic carbon. *Biogeosciences*, 13, 4167-4185, doi: 10.5194/bg-13-4167-2016.,
527 2016
528
- 529 Brandon, M., Goyet, C., Touratier, F., Lefèvre, N., Kestenare, E., and Morrow, R.: Spatial and temporal
530 variability of the physical, carbonate and CO₂ properties in the Southern Ocean surface waters
531 during austral summer (2005-2019), *Deep-Sea Research Part I*,
532 <https://doi.org/10.1016/j.dsr.2022.103836>, 2022
533
- 534 Brévière, E., N.Metzl, A.Poisson and B.Tilbrook, 2006. Changes of oceanic CO₂ sink in the Eastern
535 Indian sector of the Southern Ocean. *Tellus*, 58B, 438-446, 10.1111/j.1600-0889.2006.00220.x
536
- 537 Carter, B. R., Williams, N. L., Gray, A. R., and Feely, R. A.: Locally interpolated alkalinity regression for
538 global alkalinity estimation. *Limnol. Oceanogr.: Methods* 14: 268–277. doi:10.1002/lom3.10087,
539 2016



- 540
541 Carter, B. R., Feely, R. A., Williams, N. L., Dickson, A. G., Fong, M. B., and Takeshita, Y.: Updated
542 methods for global locally interpolated estimation of alkalinity, pH, and nitrate. *Limnology and*
543 *Oceanography: Methods*, 16: 119-131. doi: 10.1002/lom3.10232, 2017
544
545 Carter, B.R., Feely, R.A., Wanninkhof, R., Kouketsu, S., Sonnerup, R.E., Pardo, P.C., Sabine, C.L.,
546 Johnson, G.C., Sloyan, B.M., Murata, A., Mecking, S., Tilbrook, B., Speer, K., Talley, L.D., Millero, F.J.,
547 Wijffels, S.E., Macdonald, A.M., Gruber, N., Bullister, J.L., 2019. Pacific anthropogenic carbon
548 between 1991 and 2017. *Global Biogeochem. Cycles* 33, 597–617.
549 <https://doi.org/10.1029/2018GB006154>.
550
551 Chau, T.-T.-T., Gehlen, M., Metzl, N., and Chevallier, F.: CMEMS-LSCE: a global, 0.25°, monthly
552 reconstruction of the surface ocean carbonate system, *Earth Syst. Sci. Data*, 16, 121–160,
553 <https://doi.org/10.5194/essd-16-121-2024>, 2024.
554
555 Cheng, L., Abraham, J., Trenberth, K.E. et al. Record High Temperatures in the Ocean in 2024. *Adv.*
556 *Atmos. Sci.* 42, 1092–1109. <https://doi.org/10.1007/s00376-025-4541-3>, 2025.
557
558 Deng, P., He, S., Zhang, Z., Smith, W. O., Jr., He, J., Lan, M., et al.: Increased carbon sink within the
559 seasonal sea ice zone associated with climate variability in the Southern Ocean. *Geophysical*
560 *Research Letters*, 52, e2025GL118274. <https://doi.org/10.1029/2025GL118274>, 2025
561
562 Dickson, A. G., 1990. Standard potential of the reaction: $\text{AgCl(s)} + \frac{1}{2}\text{H}_2(\text{g}) = \text{Ag(s)} + \text{HCl(aq)}$, and the
563 standard acidity constant of the ion HSO_4^- in synthetic sea water from 273.15 to 318.15 K. *J. Chem.*
564 *Thermodyn.* 22: 113–127. doi:10.1016/0021-9614(90)90074-Z.
565
566 Dickson, A. G., Sabine, C. L., and Christian, J. R.: Guide to best practices for ocean CO₂
567 measurements, North Pacific Marine Science Organization, Sidney, British Columbia, 191,
568 <https://doi.org/10.25607/OBP-1342>, 2007.
569
570 Duncan, R.J., Nielsen, D.A., Sheehan, C.E., Deppeler, S., Hancock, A.M., Schulz, K.G., Davidson, A.T.
571 and Petrou, K.: Ocean acidification alters the nutritional value of Antarctic diatoms. *New Phytol*, 233:
572 1813-1827. <https://doi-org.insu.bib.cnrs.fr/10.1111/nph.17868>, 2022
573
574 Edmond, J.M.: High precision determination of titration alkalinity and total carbon dioxide content of
575 sea water by potentiometric titration. *Deep-Sea Res.* 17, 737–750. [https://doi.org/10.1016/0011-](https://doi.org/10.1016/0011-7471(70)90038-0)
576 [7471\(70\)90038-0](https://doi.org/10.1016/0011-7471(70)90038-0), 1970
577
578 Fay, A. R., Munro, D. R., McKinley, G. A., Pierrot, D., Sutherland, S. C., Sweeney, C., and Wanninkhof,
579 R.: Updated climatological mean ΔfCO_2 and net sea–air CO₂ flux over the global open ocean regions,
580 *Earth Syst. Sci. Data*, 16, 2123–2139, <https://doi.org/10.5194/essd-16-2123-2024>, 2024.
581
582 Gordon, A. L., and Tchernia, P. L.: Waters of the continental margin off Adelle Coast, Antarctica.
583 *Antarctica Oceanology II: The Australian-New Zealand Sector*, 59-69, 1972
584



- 585 Hauck J., Hoppema, M., Bellerby, R. G. J., Völker, C., and Wolf-Gladrow, D.: Data-based estimation of
586 anthropogenic carbon and acidification in the Weddell Sea on a decadal timescale. *J. Geophys. Res.*
587 115, C03004. doi:10.1029/2009jc005479, 2010
588
- 589 Ishii, M., Inoue, H. Y., and Matsueda, H.: Net community production in the marginal ice zone and its
590 importance for the variability of the oceanic pCO₂ in the Southern Ocean south of Australia. *Deep*
591 *Sea Research Part II: Topical Studies in Oceanography*, 49(9), 1691–1706.
592 [https://doi.org/10.1016/s0967-0645\(02\)00007-3](https://doi.org/10.1016/s0967-0645(02)00007-3), 2002
593
- 594 Jiang, L.-Q., Dunne, J., Carter, B. R., Tjiputra, J. F., Terhaar, J., Sharp, J. D., et al.: Global surface ocean
595 acidification indicators from 1750 to 2100. *Journal of Advances in Modeling Earth Systems*, 15,
596 e2022MS003563. <https://doi.org/10.1029/2022MS003563>, 2023
597
- 598 Laika, H. E., Goyet C., Vouve F., Poisson A., and Touratier F.: Interannual properties of the CO₂ system
599 in the Southern Ocean south of Australia. *Antarctic Science*, 21(6), 663–680.
600 <https://doi.org/10.1017/S0954102009990319>, 2009
601
- 602 Landschützer, P., Gruber, N., Bakker, D. C. E., Stemmler, I., and Six, K. D.: Strengthening seasonal
603 marine CO₂ variations due to increasing atmospheric CO₂. *Nature Climate Change*, 8(2), 146–150.
604 <https://doi.org/10.1038/s41558-017-0057-x>, 2018
605
- 606 Laruelle, G.G., Cai, W.-J., Hu, X., Gruber, N., Mackenzie, F.T., and Regnier, P.: Continental shelves as a
607 variable but increasing global sink for atmospheric carbon dioxide. *Nat. Commun.* 9, 454, DOI:
608 10.1038/s41467-017-02738-z, 2018
609
- 610 Lauvset, S. K., Lange, N., Tanhua, T., Bittig, H. C., Olsen, A., Kozyr, A., Álvarez, M., Azetsu-Scott, K.,
611 Brown, P. J., Carter, B. R., Cotrim da Cunha, L., Hoppema, M., Humphreys, M. P., Ishii, M., Jeansson,
612 E., Murata, A., Müller, J. D., Pérez, F. F., Schirnack, C., Steinfeldt, R., Suzuki, T., Ulfssbo, A., Velo, A.,
613 Woosley, R. J., and Key, R. M.: The annual update GLODAPv2.2023: the global interior ocean
614 biogeochemical data product, *Earth Syst. Sci. Data*, 16, 2047–2072, [https://doi.org/10.5194/essd-16-](https://doi.org/10.5194/essd-16-2047-2024)
615 2047-2024, 2024.
616
- 617 Lauvset, Siv K.; Lange, Nico; Tanhua, Toste; Bittig, Henry C.; Olsen, Are; Kozyr, Alex; Álvarez, Marta;
618 Azetsu-Scott, Kumiko; Becker, Susan; Brown, Peter J.; Carter, Brendan R.; Cotrim da Cunha, Leticia;
619 Feely, Richard A.; Hoppema, Mario; Humphreys, Matthew P.; Ishii, Masao; Jeansson, Emil; Jones,
620 Steve D.; Lo Monaco, Claire; Murata, Akihiko; Müller, Jens Daniel; Pérez, Fiz F.; Schirnack, Carsten;
621 Steinfeldt, Reiner; Suzuki, Toru; Tilbrook, Bronte; Ulfssbo, Adam; Velo, Antón; Woosley, Ryan J.; Key,
622 Robert M.: Global Ocean Data Analysis Project version 2.2023 (GLODAPv2.2023) (NCEI Accession
623 0283442). [indicate subset used]. NOAA National Centers for Environmental Information. Dataset.
624 <https://doi.org/10.25921/zyrq-ht66>. Last Access [4 June 2025], 2023
625
- 626 Lee, K., Tong, L. T., Millero, F. J., Sabine, C. L., Dickson, A. G., Goyet, C., Park, G. H., Wanninkhof, R.,
627 Feely, R. A., and Key, R. M.: Global relationships of total alkalinity with salinity and temperature in
628 surface waters of the world's oceans. *Geophys. Res. Lett.* 33, L19605. doi:10.1029/2006GL027207,
629 2006.



- 630
- 631 Leseurre, C., Lo Monaco, C., Reverdin, G., Metzl, N., Fin, J., Mignon, C., and Benito, L.: Summer trends
632 and drivers of sea surface fCO₂ and pH changes observed in the southern Indian Ocean over the last
633 two decades (1998–2019), *Biogeosciences*, 19, 2599–2625, [https://doi.org/10.5194/bg-19-2599-](https://doi.org/10.5194/bg-19-2599-2022)
634 2022, 2022.
- 635
- 636 Lueker, T.J., Dickson, A.G., Keeling, C.D.: Ocean pCO₂ calculated from dissolved inorganic carbon,
637 alkalinity, and equations for K-1 and K-2: validation based on laboratory measurements of CO₂ in gas
638 and seawater at equilibrium. *Marine Chemistry* 70, 105-119. [https://doi.org/10.1016/S0304-](https://doi.org/10.1016/S0304-4203(00)00022-0)
639 4203(00)00022-0, 2000
- 640
- 641 Mahieu, L., Lo Monaco, C., Metzl, N., Fin, J., and Mignon, C.: Variability and stability of anthropogenic
642 CO₂ in Antarctic Bottom Water observed in the Indian sector of the Southern Ocean, 1978–2018,
643 *Ocean Sci.*, 16, 1559–1576, <https://doi.org/10.5194/os-16-1559-2020>, 2020.
- 644
- 645 Mazloff, M. R., Verdy, A., Gille, S. T., Johnson, K. S., Cornuelle, B. D., and Sarmiento, J.: Southern
646 Ocean acidification revealed by biogeochemical-Argo floats. *Journal of Geophysical Research: Oceans*, 128, e2022JC019530. <https://doi.org/10.1029/2022JC019530>, 2023.
- 647
- 648
- 649 McNeil, B. I., Tilbrook, B. and Matear, R. J.: Accumulation and uptake of anthropogenic CO₂ in the
650 Southern Ocean, south of Australia between 1968 and 1996, *J. Geophys. Res.*, 106, 31,431– 31,445,
651 2001
- 652
- 653 Meinshausen, M., Nicholls, Z. R. J., Lewis, J., Gidden, M. J., Vogel, E., Freund, M., et al.: The shared
654 socioeconomic pathway (SSP) greenhouse gas concentrations and their extensions to 2500.
655 *Geoscientific Model Development*, 13(8), 3571–3605. <https://doi.org/10.5194/gmd-13-3571-2020>,
656 2020.
- 657
- 658 Metzl, N., B. Tilbrook and A. Poisson: The annual fCO₂ cycle and the air-sea CO₂ flux in the sub-
659 Antarctic Ocean. *Tellus*, 51B, 4, 849-861. <https://doi.org/10.1034/j.1600-0889.1999.t01-3-00008.x>,
660 1999.
- 661
- 662 Metzl Nicolas, Fin Jonathan, Lo Monaco Claire, Mignon Claude, Alliouane Samir, Bombled Bruno,
663 Boutin Jacqueline, Bozec Yann, Comeau Steeve, Conan Pascal, Coppola Laurent, Cuet Pascale,
664 Ferreira Eva, Gattuso Jean-Pierre, Gazeau Frédéric, Goyet Catherine, Grossteffan Emilie, Lansard
665 Bruno, Lefèvre Dominique, Lefèvre Nathalie, Leseurre Coraline, Lombard Fabien, Petton Sébastien,
666 Pujo-Pay Mireille, Rabouille Christophe, Reverdin Gilles, Ridame Céline, Rimmelin-Maury Peggy,
667 Ternon Jean-François, Touratier Franck, Tribollet Aline, Wagener Thibaut, Wimart-Rousseau Cathy:
668 An updated synthesis of ocean total alkalinity and dissolved inorganic carbon measurements from
669 1993 to 2023: the SNAPO-CO₂-v2 dataset. *SEANOE*. <https://doi.org/10.17882/102337>, 2024a.
- 670
- 671 Metzl, N., Lo Monaco, C., Leseurre, C., Ridame, C., Reverdin, G., Chau, T. T. T., Chevallier, F., and
672 Gehlen, M.: Anthropogenic CO₂, air–sea CO₂ fluxes, and acidification in the Southern Ocean: results
673 from a time-series analysis at station OISO-KERFIX (51° S–68° E), *Ocean Sci.*, 20, 725–758,
674 <https://doi.org/10.5194/os-20-725-2024>, 2024b.



675
676 Metzl, N., Fin, J., Lo Monaco, C., Mignon, C., Alliouane, S., Bombled, B., Boutin, J., Bozec, Y., Comeau,
677 S., Conan, P., Coppola, L., Cuet, P., Ferreira, E., Gattuso, J.-P., Gazeau, F., Goyet, C., Grossteffan, E.,
678 Lansard, B., Lefèvre, D., Lefèvre, N., Leseurre, C., Petton, S., Pujo-Pay, M., Rabouille, C., Reverdin, G.,
679 Ridame, C., Rimmelin-Maury, P., Ternon, J.-F., Touratier, F., Tribollet, A., Wagener, T., and Wimart-
680 Rousseau, C.: An updated synthesis of ocean total alkalinity and dissolved inorganic carbon
681 measurements from 1993 to 2023: the SNAPO-CO₂-v2 dataset, *Earth Syst. Sci. Data*, 17, 1075–1100,
682 <https://doi.org/10.5194/essd-17-1075-2025>, 2025a.
683
684 Metzl, N., Lo Monaco, C., Tribollet, A., Ternon, J.-F., Chevallier, F., and Gehlen, M.: New observations
685 confirm the progressive acidification in the Mozambique Channel, *Biogeosciences*, 22, 7187–7204,
686 <https://doi.org/10.5194/bg-22-7187-2025>, 2025b.
687
688 Midorikawa, T., Inoue, H. Y., Ishii, M., Sasano, D., Kosugi, N., Hashida, G., Nakaoka, S., and Suzuki, T.:
689 Decreasing pH trend estimated from 35-year time series of carbonate parameters in the Pacific
690 sector of the Southern Ocean in summer, *Deep-Sea Res.*, 61, 131–139,
691 <https://doi.org/10.1016/j.dsr.2011.12.003>, 2012.
692
693 Millero, F. J., Lee, K., Roche, M.: Distribution of alkalinity in the surface waters of the major oceans.
694 *Mar. Chem.* 60, 111–130. [https://doi.org/10.1016/S0304-4203\(97\)00084-4](https://doi.org/10.1016/S0304-4203(97)00084-4), 1998
695
696 Morrow, R. and Kestenare, E.: 30 years of sea surface temperature and salinity observations crossing
697 the Southern Ocean near 140°E: Trends and rollercoaster variability, *Journal of Marine System*,
698 <https://doi.org/10.1016/j.jmarsys.2025.104048>, 2025.
699
700 Munro, D. R., N. S. Lovenduski, T. Takahashi, B. B. Stephens, T. Newberger, and C. Sweeney: Recent
701 evidence for a strengthening CO₂ sink in the Southern Ocean from carbonate system measurements
702 in the Drake Passage (2002–2015), *Geophys. Res. Lett.*, 42, doi:10.1002/2015GL065194, 2015.
703
704 Nissen, C., Lovenduski, N.S., Brooks, C.M. et al.: Severe 21st-century ocean acidification in Antarctic
705 Marine Protected Areas. *Nat Commun* 15, 259. <https://doi.org/10.1038/s41467-023-44438-x>, 2024.
706
707 Orr, J. C., Epitalon, J.-M., Dickson, A. G., Gattuso, J.-P.: Routine uncertainty propagation for the
708 marine carbon dioxide system, *Marine Chemistry*, Vol. 207, 84–107,
709 doi:10.1016/j.marchem.2018.10.006., 2018.
710
711 Petrou, K., Baker, K. G., Nielsen, D. A., Hancock, A. M., Schulz, K. G. and Davidson, A. T.: Acidification
712 diminishes diatom silica production in the Southern Ocean. *Nature Climate Change*, 9, 781–786,
713 <https://doi.org/10.1038/s41558-019-0557-y>, 2019.
714
715 Pardo, P. C., Tilbrook, B., Langlais, C., Trull, T. W., and Rintoul, S. R.: Carbon uptake and
716 biogeochemical change in the Southern Ocean, south of Tasmania. *Biogeosciences*, 14(22), 5217–
717 5237. <https://doi.org/10.5194/bg-14-5217-2017>, 2017.
718



- 719 Pierrot, D., C. Neill, K. Sullivan, R. Castle, R. Wanninkhof, H. Lüger, T. Johannessen, A. Olsen, R. A.
720 Feely, C. E. Cosca: Recommendations for Autonomous Underway pCO₂ Measuring Systems and Data
721 Reduction Routines, Deep-Sea Research II, doi:10.1016/j.dsr2.2008.12.005, 2009.
722
- 723 Rodgers, K. B., Schwinger, J., Fassbender, A. J., Landschützer, P., Yamaguchi, R., Frenzel, H., et al.:
724 Seasonal variability of the surface ocean carbon cycle: A synthesis. *Global Biogeochemical Cycles*, 37,
725 e2023GB007798. <https://doi.org/10.1029/2023GB007798>, 2023.
726
- 727 Roobaert, A., Resplandy, L., Laruelle, G. G., Liao, E., and Regnier, P. : Unraveling the physical and
728 biological controls of the global coastal CO₂ sink. *Global Biogeochemical Cycles*, 38, e2023GB007799.
729 <https://doi.org/10.1029/2023GB007799>, 2024a.
730
- 731 Roobaert, A., Regnier, P., Landschützer, P., and Laruelle, G. G.: A novel sea surface pCO₂-product for
732 the global coastal ocean resolving trends over 1982–2020, *Earth Syst. Sci. Data*, 16, 421–441,
733 <https://doi.org/10.5194/essd-16-421-2024>, 2024b.
734
- 735 Shadwick, E., Rintoul, S., Tilbrook, B., Williams, G., Young, N., Fraser, A. D., et al.: Glacier tongue
736 calving reduced dense water formation and enhanced carbon uptake. *Geophysical Research Letters*,
737 40(5), 904–909. <https://doi.org/10.1002/grl.50178>, 2013.
738
- 739 Shadwick, E. H., B. Tilbrook, and G. D. Williams: Carbonate chemistry in the Mertz Polynya (East
740 Antarctica): Biological and physical modification of dense water outflows and the export of
741 anthropogenic CO₂, *J. Geophys. Res. Oceans*, 119, 1–14, doi:10.1002/2013JC009286, 2014.
742
- 743 Shadwick, E. H., B. Tilbrook, and K. I. Currie: Late-summer biogeochemistry in the Mertz Polynya: East
744 Antarctica, *J. Geophys. Res. Oceans*, 122, 7380–7394, doi:10.1002/2017JC013015, 2017.
745
- 746 Shadwick, E. H., Wynn-Edwards, C. A., Matear, R.J., Jansen, P., Schulz, E. and Sutton, A. J.: Observed
747 amplification of the seasonal CO₂ cycle at the Southern Ocean Time Series. *Front. Mar. Sci.*
748 10:1281854. doi: 10.3389/fmars.2023.1281854, 2023.
749
- 750 Schlitzer, R.: Ocean Data View, <http://odv.awi.de>, 2018.
751
- 752 Sholeninova, P., Morrison, A. K., McC. Hogg, A., and Foppert, A. :Quantification of Antarctic bottom
753 water pathways in the Australian-Antarctic Basin. *Journal of Geophysical Research: Oceans*, 130,
754 e2024JC022305. <https://doi.org/10.1029/2024JC022305>, 2025
755
- 756 Stark, J., S., et al.: Carbonate chemistry of an in-situ free-ocean CO₂ enrichment experiment
757 (antFOCE) in comparison to short term variation in Antarctic coastal waters. *Scientific Reports*,
758 8:2816, DOI:10.1038/s41598-018-21029-1., 2018.
759
- 760 Takahashi, T., Sutherland, S.C., Chipman, D.W., Goddard, J.G., Ho, C., Newberger, T., Sweeney, C.,
761 Munro, D.R.: Climatological distributions of pH, pCO₂, total CO₂, alkalinity, and CaCO₃ saturation in
762 the global surface ocean, and temporal changes at selected locations. *Mar. Chem.* 164, 95–125.
763 <https://doi.org/10.1016/j.marchem.2014.06.004>, 2014



764
765 Tilbrook, B., E. B. Jewett, M. D. DeGrandpre, J. M. Hernandez-Ayon, R. A. Feely, D. K. Gledhill, L.
766 Hansson, K. Isensee, M. L. Kurz, J. A. Newton, S. A. Siedlecki, F. Chai, S. Dupont, M. Graco, E. Calvo, D.
767 Greeley, L. Kapsenberg, M. Lebrech, C. Pelejero, K. L. Schoo, M. Telszewski: An Enhanced Ocean
768 Acidification Observing Network: From People to Technology to Data Synthesis and Information
769 Exchange. *Frontiers in Marine Science*, 6, 337, DOI:10.3389/fmars.2019.00337, 2019.
770
771 Tilbrook, B., C. Neill and J. Akl: Surface water CO₂ measurements from ships of opportunity: A report
772 for Australia's Integrated Marine Observing System, 26p., doi: 10.25919/x90f-bw32, 2025.
773
774 Touratier, F., Azouzi, L., and Goyet, C.: CFC-11, $\Delta 14\text{C}$ and 3H tracers as a means to assess
775 anthropogenic CO₂ concentrations in the ocean. *Tellus B*, 59(2), 318–325, doi:10.1111/j.1600-
776 0889.2006.00247.x., 2007.
777
778 Uppström, L. R.: The boron/chlorinity ratio of deep-sea water from the Pacific Ocean, *Deep Sea*
779 *Research and Oceanographic Abstracts*, 21, 161–162, [https://doi.org/10.1016/0011-7471\(74\)90074-](https://doi.org/10.1016/0011-7471(74)90074-6)
780 *6.*, 1974.
781
782 van Wijk, E. M., and Rintoul, S. R.: Freshening drives contraction of Antarctic bottom water in the
783 Australian Antarctic Basin: Freshening drives contraction of AABW. *Geophysical Research Letters*,
784 41(5), 1657–1664. <https://doi.org/10.1002/2013GL058921>, 2014
785
786 Williams, G. D., Aoki, S., Jacobs, S. S., Rintoul, S. R., Tamura, T., and Bindoff, N. L.: Antarctic Bottom
787 Water from the Adélie and George V Land coast, East Antarctica (140–149 E), *J. Geophys. Res.-*
788 *Ocean.*, 115, C04027, <https://doi.org/10.1029/2009JC005812>, 2010.
789
790 Xue, L., Cai, W. J., Takahashi, T. et al.: Climatic modulation of surface acidification rates through
791 summertime wind forcing in the Southern Ocean. *Nat. Commun.*, 9, 3240, Doi:10.1038/s41467-018-
792 05443-7, 2018.
793
794 Zhang, S., Wu, Y., Cai, W.-J., Cai, W., Feely, R. A., Wang, Z., et al.: Transport of anthropogenic carbon
795 from the Antarctic shelf to deep Southern Ocean triggers acidification. *Global Biogeochemical Cycles*,
796 37, e2023GB007921. <https://doi.org/10.1029/2023GB007921>, 2023.
797



798 Tables :

799

800 Table 1: Trends of properties in the Adélie zone derived from observations (measured A_T , C_T or fCO_2) and from
 801 the FFNN model. For observations the trends are evaluated for summer only. For the FFNN model trends are
 802 estimated for all seasons or only for January and August. The last line is based on winter data in 2024 (BGC-
 803 Argo) and 1996 (A_T C_T data). Standard-deviations are in brackets.

804

805 Method	806 Period	fCO_2 $\mu atm.yr^{-1}$	A_T $\mu mol.kg.yr^{-1}$	C_T $\mu mol.kg.yr^{-1}$	pH_T yr^{-1}	Ωar yr^{-1}
809 A_T C_T 1995-2025		0.14	-0.11	0.00	-0.0002	-0.0010
810 Summer		(0.66)	(0.38)	(0.36)	(0.0008)	(0.0027)
812 fCO_2 1984-2025		1.33	0.04	0.50	-0.0015	-0.0040
813 Summer		(0.33)	(0.25)	(0.24)	(0.0004)	(0.0011)
815 FFNN 1985-2025		0.58	-0.29	0.08	-0.0007	-0.0031
816 Summer		(0.23)	(0.08)	(0.15)	(0.0003)	(0.0010)
818 FFNN 1985-2025		1.33	-0.002	0.44	-0.0013	-0.0035
819 Winter		(0.04)	(0.007)	(0.01)	(0.0001)	(0.0001)
821 FFNN 1985-2024		1.27	-0.05	0.44	-0.0013	-0.0040
822 Annual		(0.09)	(0.04)	(0.08)	(0.0001)	(0.0003)
824 BGC-Argo versus A_T C_T 825 Winter 2024 versus 1996		2.28	-0.27	0.50	-0.0028	-0.0063

826

827

828

829



830

831 Table 2: Trends of properties (per year) in layers 100-150m, 150-200m and 200-250m for 1995-2024. Standard-
832 deviations are in bracket. (*) indicates results without the 2013 anomaly. (**) indicates results without the
833 2013 anomaly and without the 2024 BGC-Argo data.

834

835 Layer	T	Sal	O ₂	A _T	C _T	C _{ant}
836	°C.yr ⁻¹	psu.yr ⁻¹	μmol.kg.yr ⁻¹	μmol.kg.yr ⁻¹	μmol.kg.yr ⁻¹	μmol.kg.yr ⁻¹
837						
838 100-150m	-0.018	-0.002	0.37	-0.05	0.29	0.37
839	0.035	0.001	1.07	0.11	0.21	0.18
840						
841 100-150m*	-0.030	-0.002	0.75	-0.05	0.21	0.42
842	0.027	0.001	0.77	0.12	0.15	0.15
843						
844 100-150m**	-0.030	-0.001	1.05	0.10	0.15	0.50
845 (1995-2018)	0.039	0.001	1.08	0.14	0.21	0.20
846						
847 150-200m	-0.026	-0.003	0.64	-0.07	0.16	0.37
848	0.038	0.001	1.21	0.12	0.24	0.23
849						
850 200-250m	-0.011	-0.001	0.14	0.03	0.34	0.28
851	0.039	0.001	1.25	0.10	0.24	0.25

852

853



854

855

856 Table 3: Sea surface values of properties in winter for different years and methods in the Adélie Land
 857 region (Figure 12). Methods are from observations (Obs.), FFNN model (FFNN) and reconstructions
 858 based on two scenarios SSP2-4.5 (SSP45) and SSP2-8.5 (SSP85). For C_{ant} the value is for the layer 100-
 859 150m. The last line is for year 2090 using SSP2-85 scenario.

860

861

862	Method	Year	Atm. CO ₂	fCO ₂	C _T	pH _T	Ω _{ar}	C _{ant}
863			ppm	μatm	μmol.kg ⁻¹	-	-	μmol.kg ⁻¹
864	Obs. AT CT	1996	357.6	377.3	2196.3	8.052	1.319	22.3
865	FFNN	1996	357.6	386.4	2198.3	8.048	1.335	
866	FFNN	2024	417.9	427.0	2213.9	8.008	1.230	
867	FFNN	2025	421.6	427.6	2214.5	8.007	1.229	
868	Obs. BGC	2024	428.2	431.6	2219.4	7.986	1.180	36.3
869	SSP 85	2024	428.2	417.3	2212.0	8.013	1.218	38.3
870	SSP 45	2024	426.1	416.1	2211.6	8.014	1.221	37.9
871	SSP 85	2040	500.0	460.7	2224.8	7.973	1.120	51.2
872	SSP 45	2040	475.3	445.2	2220.4	7.987	1.153	46.7
873	SSP 85	2055	600.4	531.6	2242.8	7.916	0.991	69.2
874	SSP 45	2055	522.3	475.4	2228.8	7.961	1.091	55.2
875	SSP 85	2060	643.0	565.8	2250.5	7.890	0.938	76.8
876	SSP 45	2060	537.1	485.4	2231.5	7.952	1.071	57.8
877	SSP 85	2080	864.4	789.1	2290.2	7.754	0.698	116.5
878	SSP 45	2080	585.1	520.0	2240.1	7.925	1.010	66.4
879	SSP 85	2090	998.3	965.7	2314.2	7.670	0.581	140.5

880

881

882

883



884

885 Figure 1: Maps of (a) SOCAT data and (b) GLODAP data selected in the Adélie Land region. Color code
886 is for year. Figures produced with ODV (Schlitzer, 2018).

887

888

889

890

891

892

893

894

895

896

897

898

899

900

901

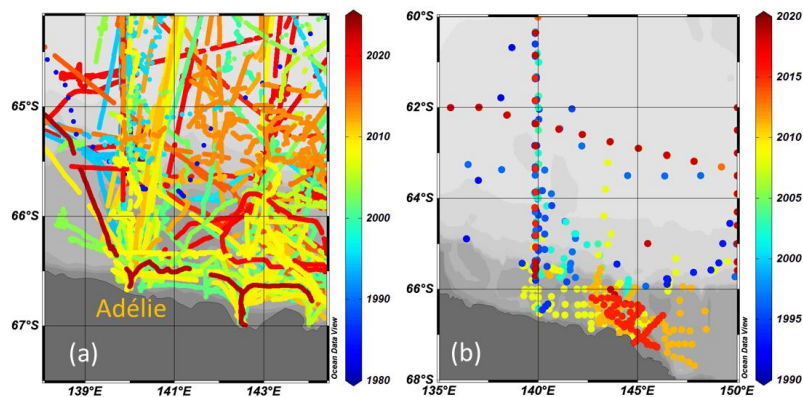
902

903

904

905

906





907

908

Figure 2: Time-series of air-sea CO₂ flux (annual in black, 36-month running mean in red) in the Adélie Land region based on the FFNN-LSCE model over 1985-2025 (centered at 66°S/140°E). Also shown (orange square) the climatological flux for year 2010 at the same location (Fay et al, 2024). Negative value denotes ocean CO₂ sink.

911

912

913

914

915

916

917

918

919

920

921

922

923

924

925

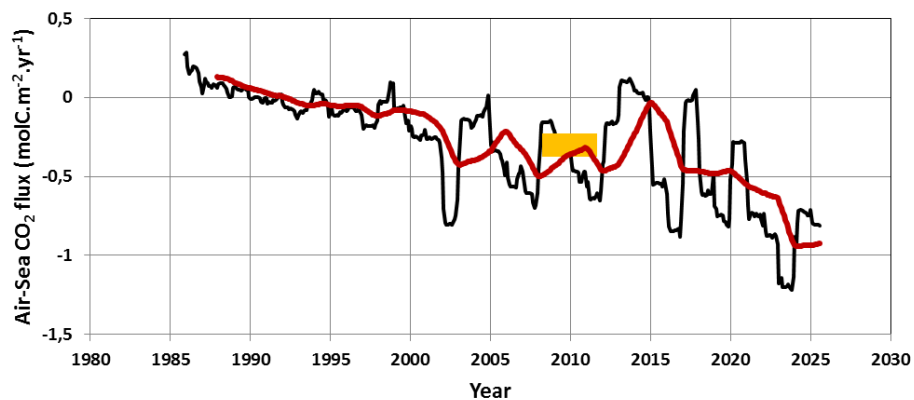
926

927

928

929

930





931

932 Figure 3: Distribution of sea surface $f\text{CO}_2$ (μatm) observed south of 65°S in January 2024 (purple) and
933 January-February 2025 (blue) from shipboard, in December 2024 and January 2025 from the BGC-
934 Argo (red diamonds), and calculated from A_T C_T data in January 2025 (orange triangles). The red
935 dashed line is the mean atmospheric CO_2 concentration in January 2025 at Cap Grim or at South Pole
936 (422 ppm). (<https://gml.noaa.gov/dv/iadv/>). Locations of the data are identified in the insert map
937 produced with ODV (Schlitzer, 2018).

938

939

940

941

942

943

944

945

946

947

948

949

950

951

952

953

954

955

956

957

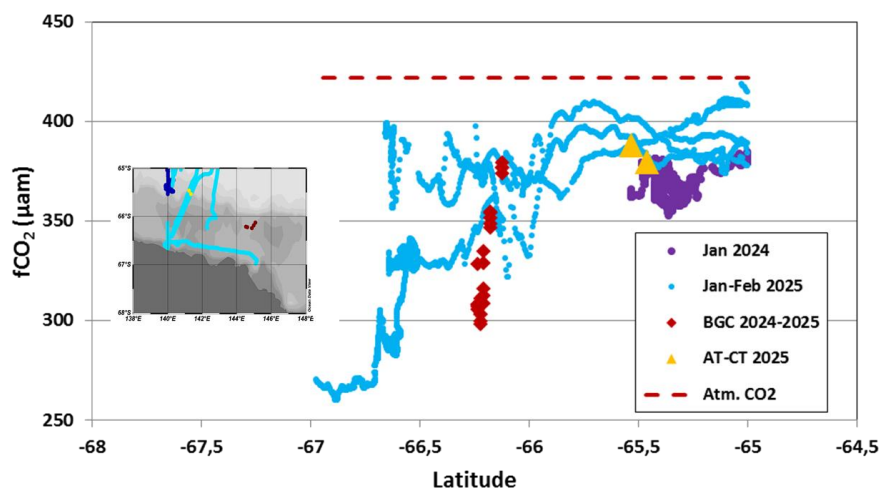
958

959

960

961

962





963

964 Figure 4: (a) Distribution of sea surface $f\text{CO}_2$ (μatm) and temperature normalized $f\text{CO}_2$ at 0°C (open
965 symbols) observed south of 65°S in January 2024 (black) and February 2025 (red) along the same
966 track. (b) Same as (a) for salinity normalized C_T concentrations ($\mu\text{mol}/\text{kg}$) calculated from $f\text{CO}_2$ data.
967 The low N-CT in 2024 ($< 2182 \mu\text{mol}/\text{kg}$) were linked to higher biological activity in 2024 (Figure S5 in
968 Supp. Mat.).

969

970

971

972

973

974

975

976

977

978

979

980

981

982

983

984

985

986

987

988

989

990

991

992

993

994

995

996

997

998

999

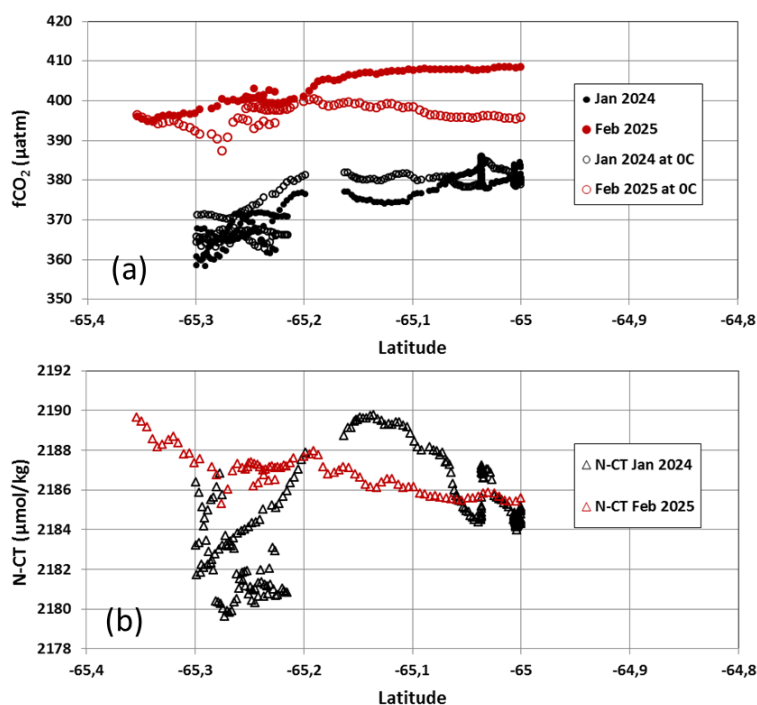
1000

1001

1002

1003

1004





1005

1006

1007

1008

1009

1010

1011

1012

1013

1014

1015

1016

1017

1018

1019

1020

1021

1022

1023

1024

1025

1026

1027

1028

1029

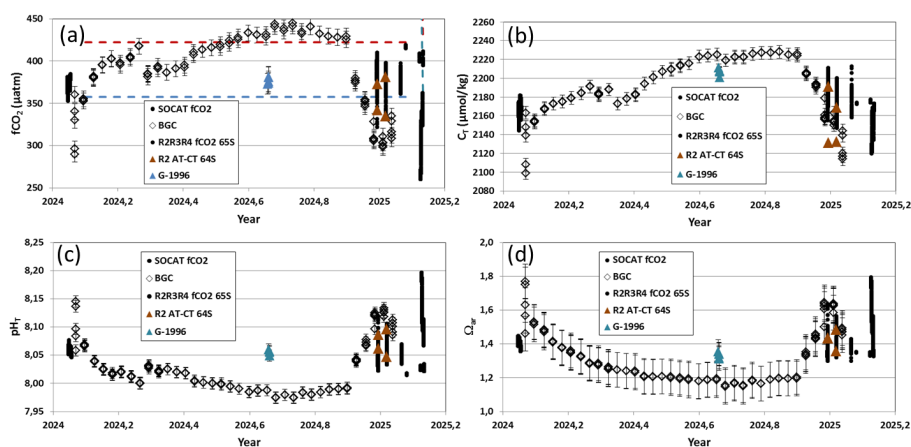
1030

1031

1032

1033

Figure 5: Time-series of (a) sea surface $f\text{CO}_2$ (μatm), (b) C_T ($\mu\text{mol/g}$), (c) pH_T and (d) Ω_{ar} observed south of 64°S in 2024-2025 based on SOCAT $f\text{CO}_2$ data (black circles), L'Astrolabe $f\text{CO}_2$ data (R2R3R4, black circles), BGC-Argo float (open diamonds) and $A_T C_T$ data in January 2025 (R2, orange triangles). Also shown the results from $A_T C_T$ data from a cruise in winter 1996 (blue triangles, cruise 09AR19960822). The dashed lines in (a) are the mean atmospheric CO_2 concentrations in 1996 (blue) and 2025 (red). Error bars (vertical) are indicated for measured or calculated values.





1034

1035

Figure 6: Time-series of (a) sea surface $f\text{CO}_2$ (μatm) and (b) C_T ($\mu\text{mol}/\text{kg}$) observed south of 65°S based on SOCAT $f\text{CO}_2$ data in summer 1985-2024 (grey circles), from $A_T C_T$ data in summer 1995-2018 (orange triangles), L'Astrolabe $f\text{CO}_2$ data in summer 2025 (R2R3R4, red circles), $A_T C_T$ data in 2025 (R2, black triangles) and BGC-Argo float data in 2024-2025 (open diamonds). Also shown are the monthly values of the FFNN model (purple) and the associated trend (dashed lines, $+1.27 \mu\text{atm}\cdot\text{yr}^{-1}$ and $0.44 \mu\text{mol}\cdot\text{kg}^{-1}\cdot\text{yr}^{-1}$). In (a) the red line is the atmospheric $f\text{CO}_2$.

1041

1042

1043

1044

1045

1046

1047

1048

1049

1050

1051

1052

1053

1054

1055

1056

1057

1058

1059

1060

1061

1062

1063

1064

1065

1066

1067

1068

1069

1070

1071

1072

1073

1074

1075

1076

1077

1078

1079

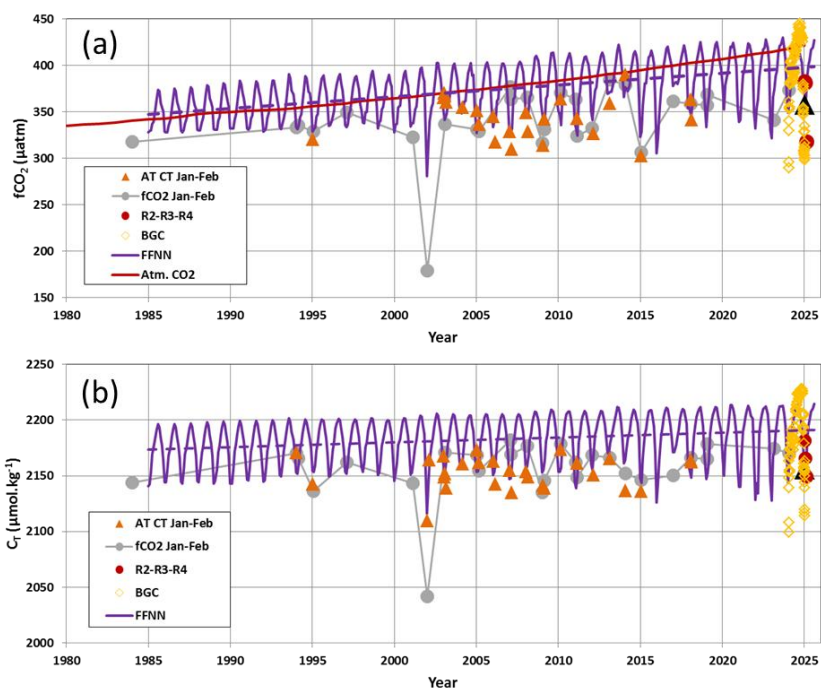
1080

1081

1082

1083

1084





1085

1086

1087

1088

1089

1090

1091

1092

1093

1094

1095

1096

1097

1098

1099

1100

1101

1102

1103

1104

1105

1106

1107

1108

1109

1110

1111

1112

1113

1114

1115

1116

1117

1118

1119

1120

1121

1122

1123

1124

1125

1126

1127

1128

1129

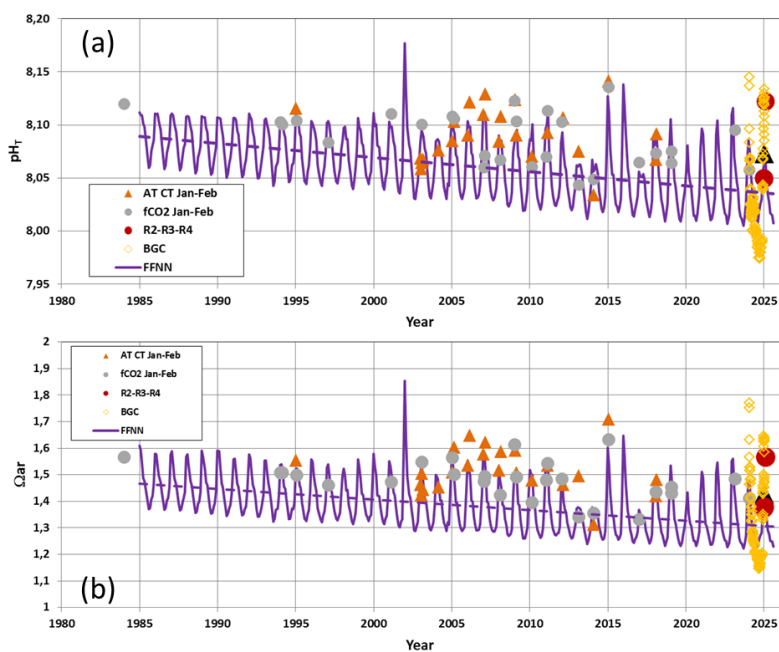
1130

1131

1132

1133

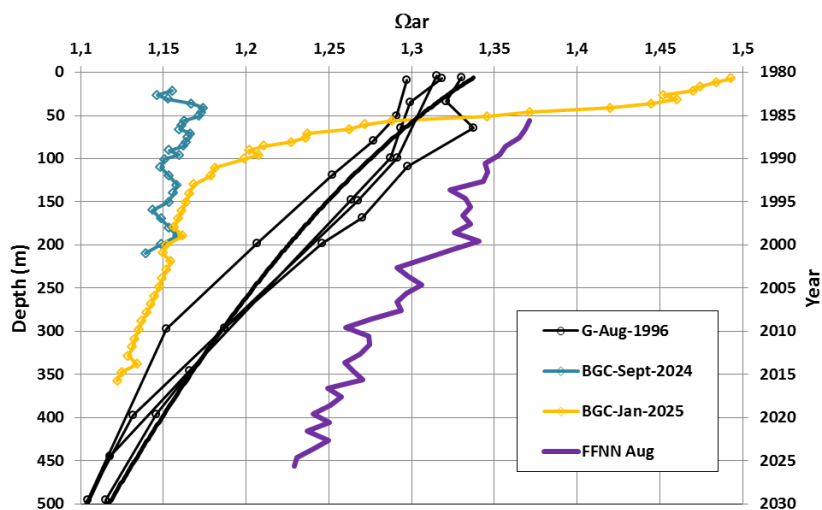
Figure 7: Time-series of (a) pH_T and (b) Ω_{ar} observed south of 65°S based on SOCAT fCO_2 data in summer 1984-2024 (grey circles), from $A_T C_T$ data in summer 1995-2018 (orange triangles), L'Astrolabe fCO_2 data in summer 2025 (R2R3R4, red circles), $A_T C_T$ data in 2025 (R2, black triangles) and BGC-Argo float data in 2024-2025 (open diamonds). Also shown are the monthly values of the FFNN model (purple) and the associated trend (dashed lines, see Table3, $pH = -0.0013.yr^{-1}$ and $\Omega_{ar} = -0.0040.yr^{-1}$).





1134
1135
1136
1137
1138
1139
1140
1141
1142
1143
1144
1145
1146
1147
1148
1149
1150
1151
1152
1153
1154
1155
1156
1157
1158
1159
1160
1161
1162
1163
1164
1165
1166
1167
1168
1169
1170
1171
1172
1173
1174
1175
1176
1177
1178
1179
1180
1181
1182
1183
1184
1185

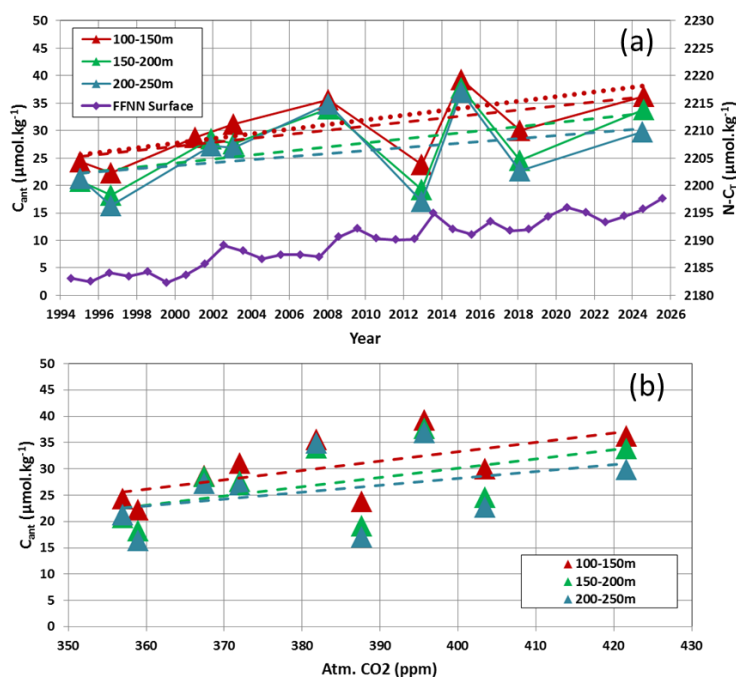
Figure 8: Profiles (0-500m left axis) of Ω_{ar} in August 1996 (GLODAP data, black circles), September 2024 (BGC-Argo, blue diamonds) and January 2025 (BGC-Argo, orange diamonds) along with surface time-series in 1985-2025 of Ω_{ar} in August from the FFNN model (purple line). In the mixed layer Ω_{ar} decreased from around 1.35 in 1996 to 1.15 in 2024 (i.e. a value observed at 300-400m in 1996). The FFNN values in August 1996 are coherent with August 1996 observations in the mixed-layer. In August 2025, Ω_{ar} FFNN value of 1.23 is close to the data observed at 200m in 1996 or at 75m in 2025 demonstrating the upward shift of Ω_{ar} .





1186
1187
1188
1189
1190
1191
1192
1193
1194
1195
1196
1197
1198
1199
1200
1201
1202
1203
1204
1205
1206
1207
1208
1209
1210
1211
1212
1213
1214
1215
1216
1217
1218
1219
1220
1221
1222
1223
1224
1225
1226
1227
1228
1229
1230
1231
1232
1233
1234
1235
1236
1237

Figure 9: (a): Time-series of anthropogenic CO₂ (C_{ant} $\mu\text{mol.kg}^{-1}$) estimated in 3 layers (below 100m) from 1994 to 2024. The C_{ant} trends are represented by dashed lines (see Table 4). Also shown the $N-C_T$ concentration ($\mu\text{mol.kg}^{-1}$, right axis) from the FFNN model in August (purple). (b): same data for C_{ant} versus atmospheric CO₂ with associated slopes (dashed lines). For the reconstructed simulation in sea surface waters the results in layer 100-150m were used with (red dashed) or without the 2013 anomaly (red dotted).





1238

1239

Figure 10: Time-series of (a) C_T concentrations, (b) atmospheric and oceanic fCO_2 , (c) pH_T and (d) Ω_{ar} based on a reconstruction for August using C_{ant} fit (red line, see Eq. 2). The reconstruction is compared with the FFNN model (purple), observations in winter 1996 and in winter 2024.

1240

1241

1242

1243

1244

1245

1246

1247

1248

1249

1250

1251

1252

1253

1254

1255

1256

1257

1258

1259

1260

1261

1262

1263

1264

1265

1266

1267

1268

1269

1270

1271

1272

1273

1274

1275

1276

1277

1278

1279

1280

1281

1282

1283

1284

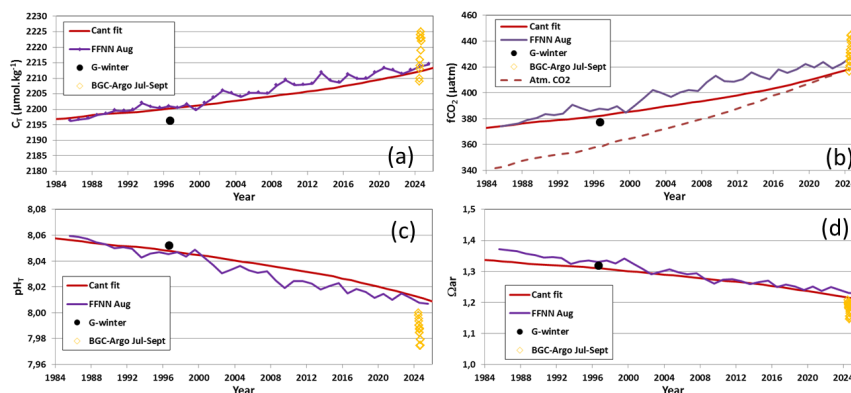
1285

1286

1287

1288

1289





1290

1291 Figure 11: Profiles of Ω_{ar} in Jan-Feb 2018 (GLODAP data, black circles) and in March 2024/January

1292 2025 (BGC-Argo, orange diamonds). Ω_{ar} saturation state ($\Omega_{ar} = 1$) occurred at depth (800-1000m) and

1293 is also identified around 100m.

1294

1295

1296

1297

1298

1299

1300

1301

1302

1303

1304

1305

1306

1307

1308

1309

1310

1311

1312

1313

1314

1315

1316

1317

1318

1319

1320

1321

1322

1323

1324

1325

1326

1327

1328

1329

1330

1331

1332

1333

1334

1335

1336

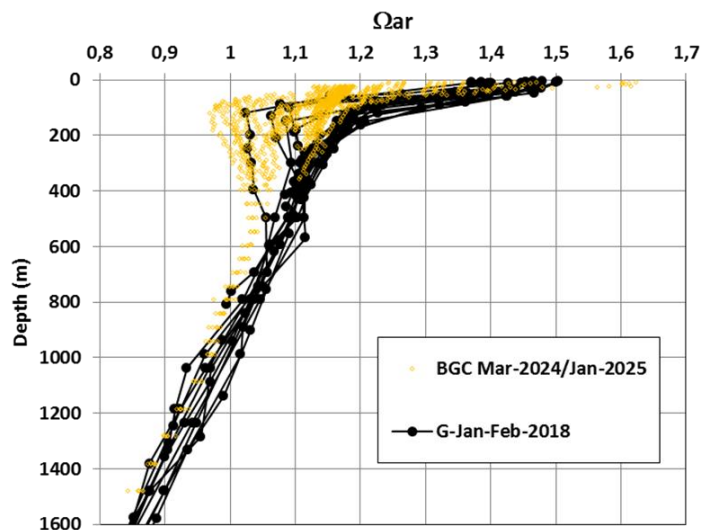
1337

1338

1339

1340

1341





1342 Figure 12: Time-series of (a) C_T concentrations, (b) pH_T and (c) Ω_{ar} on a reconstruction for August for
1343 two scenarios (SSP85, red line and SSP45 green lines). Observations in winter 1996 and 2024 and the
1344 FFNN-LSC model over 1985-2025 in August (purple) are also shown. The simulations based on C_{ant}
1345 trend with (line) or without (dashed) 2013 anomaly are presented.
1346
1347
1348
1349
1350
1351
1352
1353
1354
1355
1356
1357
1358
1359
1360
1361
1362
1363
1364
1365
1366
1367
1368
1369
1370
1371
1372
1373
1374
1375
1376
1377
1378
1379
1380
1381
1382
1383
1384
1385
1386
1387
1388
1389
1390

